



## Garnet clinopyroxenite formation via amphibole-dehydration in continental arcs: Evidence from Fe isotopes

Emma S. Sosa <sup>a,\*</sup>, Claire E. Bucholz <sup>a</sup>, Juan David Hernández-Montenegro <sup>a</sup>, Andrés Rodríguez-Vargas <sup>b</sup>, Michael A. Kipp <sup>c,1</sup>, François L.H. Tissot <sup>c</sup>

<sup>a</sup> Division of Geological and Planetary Sciences, California Institute of Technology, Pasadena, CA, 91125, United States of America

<sup>b</sup> Minerlab Limitada, Calle 51 Sur No 80i-34, 110861, Bogotá, DC, Colombia

<sup>c</sup> The Isotoparium, Division of Geological and Planetary Sciences, California Institute of Technology, Pasadena, CA, 91125, United States of America

### ARTICLE INFO

#### Keywords:

Arclogites  
Amphibole dehydration  
Cumulates  
Continental arc  
Fe isotopes  
Xenoliths

### ABSTRACT

Lower-crustal garnet clinopyroxenite (sometimes termed “arclogite”) fractionation in thick-crustal (>35 km) arc settings presents a compelling model to explain Fe-depletion trends, high oxygen fugacity, and evidence of recent delamination observed in many continental arcs. However, the origin of the garnet clinopyroxenites via igneous or metamorphic processes remains unclear. Due to the preferential incorporation of light Fe isotopes in garnet relative to clinopyroxene or amphibole, Fe isotopes are ideally suited for studying the effects of garnet fractionation on magmatic systems. Here, we present whole-rock and mineral Fe isotope data from a suite of lower to mid/upper-crustal Andean xenoliths from Mercaderes, Colombia. This data is combined with petrography, major and trace element mineral and whole-rock chemistry, geothermobarometry, and thermodynamic modeling to explore the xenoliths’ petrogenesis and the Northern Andes’ crustal structure. Whole-rock samples display a narrow range of Fe isotope compositions ( $\delta^{56}\text{Fe} = -0.02$  to  $+0.11\text{‰}$ ), which do not correlate with lithology, chemistry, or pressure-temperature conditions. This result is inconsistent with previous studies predicting the existence of an isotopically light Fe reservoir in the garnet-rich lower Andean crust. Through thermodynamic modeling, we show that the lack of isotopic fractionation in the Mercaderes xenoliths is more consistent with the suite representing a prograde metamorphic sequence, in which amphibole dehydration reactions drive metamorphism of mid/upper-crustal diorite protoliths. While our data do not preclude the presence of garnet clinopyroxenite cumulates at the base of the Andean crust, or that the delamination of such cumulates played an important role in the evolution of the Andes, they do indicate that not all garnet clinopyroxenites are cumulate in origin. Instead, the lower Andean crust represents an amalgamation of igneous and metamorphic rock, with metamorphism of mid-crustal lithologies and partial melting of mafic cumulate roots acting in tandem to drive densification and delamination of the lower crust in a self-feeding mechanism.

### 1. Introduction

Deep-crustal garnet formation in convergent margin (or arc) magmatic systems exerts a fundamental influence on processes related to continental differentiation and stability (e.g., [Kay and Kay, 1993](#); [Ducea and Saleeby, 1998](#); [Jull and Kelemen, 2001](#); [Ducea et al., 2021a, 2021b](#)). Lower-crustal garnet production results in compositional and density sorting in the crust, generating a more evolved, lower-density upper crust and an (ultra-)mafic, lower crust that may be denser than the underlying mantle and hence unstable ([Rudnick and Fountain, 1995](#)). Over the past decade, there has been renewed debate on the

effects of garnet fractionation on the development of Fe-depletion trends and the redox state of magmas from continental arcs ([Tang et al., 2018](#); [Blatter et al., 2023](#); [Holycross and Cottrell, 2023](#)). Due to the preference of garnet for  $\text{Fe}^{2+}$  relative to  $\text{Fe}^{3+}$ , it has been posited that garnet fractionation results in Fe-depleted melts with elevated  $\text{Fe}^{3+}/\Sigma\text{Fe}$  ratios ([Green and Ringwood, 1968](#); [Tang et al., 2018](#); [Du et al., 2022](#)).

Magmas from thick (>45 km) arcs have geochemistry consistent with residual garnet in their source regions (e.g.,  $\text{Sr}/Y > 40$ ,  $\text{La}/\text{Yb} > 20$ ), potentially reflecting (1) crystallization-differentiation of garnet from magmas in the uppermost mantle to lower crust (>1 GPa) (e.g., [Bryant et al., 2006](#)) or (2) partial melting of lower-crustal amphibolites and

\* Corresponding author at: Division of Geological and Planetary Sciences, California Institute of Technology, Pasadena, CA, 91125, United States of America.

<sup>1</sup> Now at Division of Earth and Climate Sciences, Duke University, Durham, North Carolina 27708.

mafic granulites forming residual or peritectic garnet (e.g., Kay and Kay, 1991). Although there is limited direct exposure or evidence of the first process, field exposures of exhumed arcs support an important role for the latter process in the formation of lower crust for both oceanic arcs such as Kohistan (Pakistan; Yamamoto and Yoshino, 1998; Yoshino and Satish-Kumar, 2001; Ringuette et al., 1999; Jagoutz et al., 2011) and continental arcs such as Fiordland (New Zealand; Daczko et al., 2001; Stowell et al., 2010).

Garnet pyroxenite xenoliths from continental arcs (i.e., “arclogites”; Lee and Anderson, 2015) also provide evidence of lower-crustal garnet-bearing cumulate or restitic assemblages. Garnet clinopyroxenites have been interpreted both as magmatic cumulates (Lee et al., 2006; Lee and Anderson, 2015; Bloch et al., 2017; Tang et al., 2018) and residues of lower-crustal melting of mafic plutonic precursors (Wyllie and Wolf, 1993; Weber et al., 2002; Bowman et al., 2021; Gianola et al., 2023). [Throughout our discussion, the terms ‘restite’ and ‘residue’ encompass all non-cumulate models in which garnet-bearing assemblages form through processes other than igneous fractionation.] As with field exposures of exhumed arcs, uncertainty in their genetic origins arises from high-temperature metamorphic re-equilibration, erasing textural and compositional information concerning their origin. However, distinguishing between these two origins is paramount for correctly interpreting their chemistry and implications for the evolution of arc magmas.

Here, we present the first Fe isotope measurements on a suite of lower to mid-crustal garnet-bearing xenoliths, including garnet clinopyroxenites, from Mercaderes, Colombia. Although we integrate petrography and mineral/whole-rock chemistry in our discussion, we focus on Fe isotopes as they are sensitive to garnet fractionation, with garnet preferentially incorporating isotopically light Fe compared to other phases (Nie et al., 2021). Previous studies have, in fact, argued that heavy Fe isotope compositions in some Andean magmas indicate that primitive arc melts experienced prolonged light Fe isotope depletion during garnet fractionation (Du et al., 2022). Using our dataset, we 1) evaluate the magmatic versus metamorphic origin of these xenoliths, leveraging the differential behavior of Fe partitioning between melts and cumulates/restites during fractional crystallization versus partial melting, and 2) discuss the implications for the Fe isotope composition of the lower to mid-Andean crust.

## 2. Geological background and previous work

The Mercaderes region is in the northern volcanic zone (NVZ) of the Central Cordillera of the Colombian Andes. The xenolith suite is hosted in the Granatifera Tuff, a pyroclastic deposit located south of the town of Mercaderes. The tuff contains xenoliths of both mantle and crustal affinities, which have been the focus of several petrographic and geochemical studies (Weber, 1998; Weber et al., 2002; Rodriguez-Vargas et al., 2005; Bloch et al., 2017; Gianola et al., 2023; Zieman et al., 2023; 2024). The lower to mid-crustal lithologies range from garnet-free gabbronorites and diorites to garnet-bearing hornblendites, clinopyroxenites, and garnetites (Weber et al., 2002; Rodriguez-Vargas et al., 2005). Common phases in these rocks include garnet, clinopyroxene, amphibole, orthopyroxene, plagioclase, and scapolite (Weber, 1998; Weber et al., 2002; Rodriguez-Vargas et al., 2005).

Weber et al. (2002) suggest that the transition from amphibole-rich lithologies to garnet clinopyroxenites represents a change from amphibolite to granulite facies metamorphism. In this framework, amphibole-bearing lithologies dehydrate along two metamorphic paths based on the presence or absence of CO<sub>2</sub>. On the CO<sub>2</sub>-free path, amphibole and plagioclase react to form clinopyroxene, garnet, and melt. In the presence of CO<sub>2</sub>, amphibole, plagioclase, and garnet could react to form clinopyroxene and scapolite. Thus, the different lithologies observed in the Mercaderes suite are considered snapshots taken at various locations along a prograde metamorphic path. The suite has subsequently been reinterpreted as primarily high-pressure igneous

cumulates (e.g., Bloch et al., 2017), though studies of andesitic to rhyolitic melt inclusions in garnets from the xenoliths support the interpretation that some are restitic (Gianola et al., 2023).

## 3. Methods

### 3.1. Petrography

Mineral modal proportions for the Mercaderes xenoliths were determined through optical petrography and micro-X-ray fluorescence (XRF) spectroscopy at Caltech. A Bruker M4 Tornado μ-XRF energy dispersive spectrometer generated phase maps from thin sections. Modal volume fractions were assumed equal to the area fractions calculated with the Bruker M4 TORNADO software using the phase cluster analysis mode (Supplemental Data, Table S1). Additional details for the XRF mapping (and all analytical methods discussed below) are given in the Supplemental Data.

### 3.2. Whole-rock chemistry

Mercaderes xenoliths selected for whole-rock analyses ( $n = 21$ ) were spheroidal and ranged from 9 to 13 cm in diameter. Altered surfaces and veining were removed with a rock saw. Samples were then cut into aliquots, crushed, and powdered with an agate grinding vessel. Powders were dried for 12 h at 110 °C to remove any absorbed water, then heated to 1050 °C for one hour to determine loss on ignition. Glass beads were prepared from the ignited powders and mixed with a Li-borate flux in a 10:1 flux: sample ratio then fused at 1200 °C. Major elements were analyzed using a Panalytical Zetium 4 kW wavelength-dispersive XRF spectrometer at Caltech following the methods in Buchholz and Spencer (2019). Trace elements were obtained from chips of glass beads through solution inductively coupled plasma mass spectrometry (ICP-MS) at Caltech following the methods of Lewis et al. (2021). These results are given in the Supplemental Data (Table S2).

### 3.3. Mineral chemistry

Major element mineral compositions of 38 Mercaderes samples were obtained using a field-emission iHP-200F electron microprobe at Caltech. A complete description of the standards used, detection limits, instrument setup, and count time for each measured element is given in the Supplemental Data (Table S3). Core and rim averages and standard deviations of each phase are given in the Supplemental Data (Tables S4-S8). For samples containing garnet and clinopyroxene, pressure and temperature were estimated with garnet-clinopyroxene geothermobarometry using the calibrations of Beyer et al. (2015) and Rava (2000). Core-to-rim electron microprobe transects of adjacent clinopyroxene-garnet pairs were used to evaluate the changes in pressure-temperature conditions recorded along these profiles. For samples containing garnet and amphibole, we also calculated temperature with garnet-amphibole thermometry (Graham and Powell, 1984). For plagioclase and amphibole-bearing samples, we used amphibole-plagioclase thermometry (Holland and Blundy, 1994) and barometry (Anderson and Smith, 1995) to calculate pressure-temperature conditions. Amphibole-only geothermobarometry (Ridolfi, 2021) was used to estimate pressure-temperature conditions for clinopyroxene hornblendites due to the lack of a phase assemblage in this lithology facilitating a thermodynamic assessment of these variables. These results were combined with whole-rock compositions to estimate densities using the *meemum* function of Perple\_X. Pressure, temperature, and density estimates for each sample are given in the Supplemental Data (Table S9).

For samples where classical thermobarometry gave unrealistic results or where precise temperature constraints were necessary to calculate mean force constants  $\langle F \rangle_{\text{amph}}$  and  $\langle F \rangle_{\text{cpx}}$  for Fe isotope modeling, we also estimated equilibrium conditions by constructing

pseudosections with Perple\_X for each whole-rock composition. From these models, endmember isopleths for garnet and clinopyroxene were extracted and compared to measured data, with the intersection of matching isopleths representing our best estimate of equilibrium conditions. These calculations are further discussed in the Supplemental Data, where model results for each sample are also given and compared to mineral equilibria thermobarometry (Supplemental Figures S1–2).

Trace element concentrations from garnet, clinopyroxene, and amphibole were obtained via laser ablation inductively coupled plasma mass spectrometry (LA-ICP-MS) at Pomona College in the David W. and Claire Oxtoby Environmental Isotope Laboratory using an Agilent 8900 triple quadrupole ICP-MS paired with an ESI NWR193 laser ablation system. Standards NIST 610 and BCR-2 were used to construct calibration curves, and Al concentrations obtained through electron microprobe analysis (EMPA) were used as an internal standard. These data were later supplemented with additional LA-ICP-MS measurements at the Resnick Water and Environment Laboratory Science at Caltech using an Agilent 8800 Triple Quadrupole ICP-MS coupled to a New Wave Research UP 193 Solid State Laser System. Mineral trace element data is given in Supplemental Data (Tables S10–S13).

### 3.4. Fe isotopes

Iron isotope compositions were obtained from whole-rock powders and mineral separates at the Isotoparium, Caltech (Supplemental Data, Table S14). Garnet, clinopyroxene, and amphibole mineral separates were hand-picked to ensure grains did not contain inclusions or show signs of alteration. Grains were sonicated in 1) isopropyl alcohol and 2) deionized water to remove surface contamination. Sample digestion and Fe purification were performed in the Isotoparium clean lab following the established methods of Dauphas et al. (2004, 2009). Samples were chemically purified alongside USGS rock powders AGV-2, BCR-2, BHVO-2, and COQ-1, whose Fe isotope compositions have been previously measured (Craddock and Dauphas, 2010), to confirm data

accuracy. Measured Fe isotope compositions of samples and USGS standards are reported in the Supplemental Data (Table S15).

Iron isotope measurements were made in wet plasma mode on a Neptune Plus (ThermoFisher) multi-collector ICP-MS. Isotopes  $^{54}\text{Fe}$ ,  $^{56}\text{Fe}$ ,  $^{57}\text{Fe}$ ,  $^{58}\text{Fe}$ ,  $^{53}\text{Cr}$ ,  $^{55}\text{Mn}$ ,  $^{59}\text{Co}$ , and  $^{60}\text{Ni}$  were measured for each sample and standard. Interferences of  $^{54}\text{Cr}$  on  $^{54}\text{Fe}$  and  $^{58}\text{Ni}$  on  $^{58}\text{Fe}$  were corrected with our  $^{53}\text{Cr}$  and  $^{60}\text{Ni}$  measurements, respectively, assuming natural isotopic abundances. We monitored  $^{55}\text{Mn}$  and  $^{59}\text{Co}$  to ensure complete matrix separation during column chemistry. Each unknown sample measurement was bracketed with the IRMM-524b metallic iron standard diluted in the same run acid and at the same Fe concentration (5 ppm, within 5%). We measured between 2 and 5 unknown and 1 to 2 USGS reference materials for each analytical run. Following the methods of Dauphas et al. (2009), we gauge instrumental uncertainty and calculate the errors reported in all figures and discussion using the standard deviation (SD) of the IRMM-524b standard for each session:

$$\text{Error} = 2 * \text{SD}_{\text{IRMM-524b}} / (n_{\text{sample}})^{0.5} \quad (1)$$

where  $n_{\text{sample}}$  is the number of replicate analyses per solution.

## 4. Results

### 4.1. Rock types and petrography

Rocks were classified with the IUGS plagioclase-pyroxene-hornblende ternary (Supplemental Figure S3). Because sample XC-MP1–1 also contains orthopyroxene, it was classified with the IUGS olivine-clinopyroxene-orthopyroxene ternary for ultramafic rocks as a garnet hornblende websterite. Neither ternary was used for rocks comprising over 75% garnet (vol%), which were classified as garnetite. The sample classification is outlined in Table 1. For discussion, we organize the Mercaderes xenoliths into six groups:

**Table 1**

Classification scheme used for Mercaderes xenoliths. The numbers and symbols in the left-hand columns correspond to the lithological groups given in Section 4.1, and the symbols for those groups are used throughout all figures. Abbreviations are: grt, garnet; cpx, clinopyroxene; opx, orthopyroxene; scp, scapolite; plag, plagioclase; and hbl, hornblende. Note that the following assemblages are classified differently in Weber et al. (2002): grt + hbl + cpx + plag: feldspar-bearing pyribolites; grt + hbl + cpx + scp: scapolite-bearing pyribolites; grt + cpx ± plag ± scp: pyrclasites/pyrigarnites.

Plotting symbol	Mineral content by group		Rock name
<i>Plagioclase/scapolite-rich</i>			
●	1 Hbl + plag		Diorite
<i>Amphibole-bearing</i>			
●	2 Hbl + cpx	Cpx < hbl	Clinopyroxene hornblendite
●	Grt + hbl + cpx + plag	Cpx < hbl, plag < 10% Cpx < hbl, plag > 10%, cpx < 5%	Plagioclase-bearing garnet hornblende clinopyroxenite Garnet hornblende gabbro
▲	Grt + hbl + cpx + scp (± plag)	Cpx < hbl, plag > 10%, cpx > 5% Cpx < hbl	Garnet clinopyroxene hornblende gabbro Scapolite-bearing garnet hornblende clinopyroxenite
■	4 Grt + hbl (± cpx)	Cpx < hbl	Garnet (± cpx) hornblendite
▲	5 Grt + hbl + cpx + opx Grt + hbl + cpx	Cpx > hbl (vol%)	Garnet hornblende websterite Garnet hornblende clinopyroxenite
<i>Amphibole-poor</i>			
●	6 Grt + cpx Grt + cpx + plag (± scp)	Grt > 75% (vol%)	Garnet clinopyroxenite Clinopyroxene garnetite

- (1) **Diorites:** Diorites ( $n = 3$ ) contain amphibole (59–62 %) and plagioclase (38–41 %), with traces of apatite and titanite (Fig. 1a).
- (2) **Clinopyroxene hornblendites:** Samples XC-MP1-3 and XC-MP1-4 are the only examples of clinopyroxene hornblendites in the xenolith suite and contain amphibole (89–90 %) and clinopyroxene (10–11 %) with traces of magnetite, apatite, and ilmenite (Fig. 1b).
- (3) **Plagioclase/scapolite-bearing garnet gabbros/clinopyroxene hornblendites:** Garnet-bearing hornblende gabbros ( $n = 3$ ) and plagioclase/scapolite-bearing garnet clinopyroxene hornblendites ( $n = 3$ ) contain amphibole (34–79 %), garnet (8–52 %),

plagioclase (0–21 %), clinopyroxene (0–19 %), scapolite (0–8 %), allanite (0–3 %), and titanite (0–3 %) with traces of rutile, magnetite, apatite, and ulvöspinel. In plagioclase-bearing hornblendite samples XC-M-4 (Fig. 1c) and XC-M-5 and scapolite-bearing hornblendite XC08-1/17, clinopyroxene is present as 200–700  $\mu\text{m}$  coronas around garnet at the garnet-amphibole interface.

- (4) **Garnet hornblendites ( $\pm \text{cpx}$ ):** These samples ( $n = 5$ ) contain amphibole (27–91 %), garnet (7–49 %), and clinopyroxene (2–28 %) with traces of rutile, apatite, and titanite (Fig. 1d). Clinopyroxene is only observed at the interface between garnet and

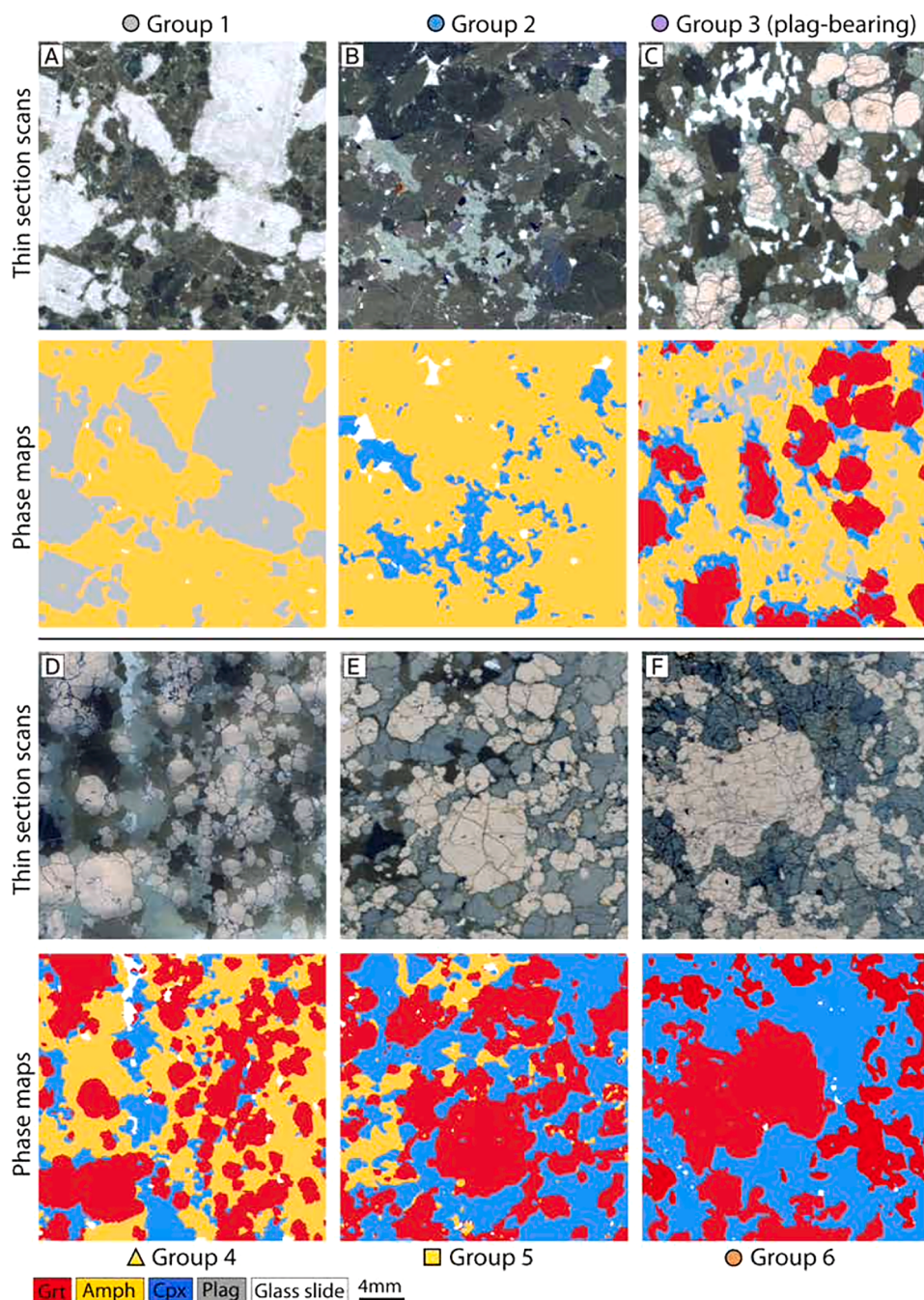


**Fig. 1.** Partial thin section scans (rows 1 and 3) and corresponding micro-XRF phase maps (rows 2 and 4) of selected Mercaderes xenoliths. A) Group 1: diorite XC-M-1. B) Group 2: clinopyroxene hornblendite XC-MP1-4. C) Group 3: plagioclase-bearing garnet clinopyroxene hornblendite XC-M-4. D) Group 4: garnet clinopyroxene hornblendite XC07-1/17. E) Group 5: garnet hornblendite clinopyroxenite XC-MG-4. F) Group 6: garnet clinopyroxenite XC-MG-2.

amphibole in garnet hornblendite samples XC-MH-8 and XC-MP2-3.

- (5) **Garnet hornblende clinopyroxenites/websterite:** These samples ( $n = 8$ ) contain clinopyroxene (21–60 %), garnet (9–57 %), amphibole (4–29 %), orthopyroxene (0–9 %), scapolite (0–2 %), and plagioclase (0–1 %) with traces of rutile, apatite, magnetite, titanite, ulvöspinel, ilmenite, and quartz (Fig. 1e). Amphibole is consistently observed as an anhedral interstitial phase, generally confined to grain boundaries between clinopyroxene and garnet. 120° triple junctures between amphibole, garnet, and clinopyroxene are common in rocks from groups 4 and 5.
- (6) **Amphibole-poor garnet clinopyroxenites/garnetite:** There are ten garnet clinopyroxenites (32–74 % garnet, 26–66 % clinopyroxene, 0–4 % amphibole) (Fig. 1f) and one plagioclase-bearing clinopyroxene garnetite (75 % garnet, 8 % plagioclase, 14 % clinopyroxene, 3 % scapolite) in our suite. Rutile is the most common accessory phase in these samples, although magnetite, ulvöspinel, titanite, and apatite are also observed.

#### 4.2. Whole-rock chemistry

Compositionally, the Mercaderes garnet clinopyroxenites ( $\pm$  amphibole) are similar to “low-MgO” ( $MgO < 13$  wt.%) pyroxenite xenoliths from the Sierra Nevada (California) and central Arizona (Dodge et al., 1988; Lee et al., 2006; Erdman et al., 2016) and to previously analyzed xenoliths from Mercaderes (Weber et al., 2002; Bloch et al., 2017; Fig. 2). Whole-rock Mg# ( $100 \times [Mg/(Mg + Fe_T)]$  molar) ranges from 42 to 69 and is positively correlated with  $SiO_2$  (38.2–49.1 wt.%). The range in Mg# and  $SiO_2$  overlap with feldspar-bearing plutonic lithologies of xenoliths from modern island arcs and of exhumed paleo-arcs (Fig. 2a), as well as calculated feldspar-bearing “cumulate” compositions from fractional crystallization experiments on hydrous basalts. (Fig. 2b). Despite their differences in phase assemblage, garnet clinopyroxenites ( $\pm$ amph) span a similar compositional range to the plagioclase and scapolite-bearing garnet clinopyroxene hornblendites

and gabbros in terms of Mg# and other major elements, with no apparent correlation between composition and sample lithology. Enrichment in the heavy rare earth elements (HREE) relative to the light heavy rare earth elements (LREE) is only observed in the garnet clinopyroxenite xenoliths (Group 6; La/Yb = 0.1–0.6, Sm/Yb = 0.3–0.4), while enrichment in the LREE relative to the HREE is only observed in hornblendite and diorite xenoliths (La/Sm = 1.0–4.4, La/Yb = 1.0–18.3) (Supplemental Figure S4).

#### 4.3. Mineral chemistry

**Garnet:** Although core-to-rim zoning is not observed in garnets from Group 6, it is present in ~80 % of samples from groups 3, 4, and 5. These samples show core-to-rim decreases in the spessartine component ( $X_{sp}$ ; −0.1 to −4 %) and increases in the pyrope component ( $X_{pyr}$ ; +0.2 to +14 %) (e.g., Fig. 3a, b). Core Mg# ranges from 22.7 to 64.1 and is highest in the Group 6 samples (40.6 – 64.1). The plagioclase and scapolite-bearing lithologies (Group 3) have the lowest core garnet pyrope component ( $X_{pyr}$  15–33 %) and highest core spessartine component ( $X_{sp}$  0.8–5 %; Fig. 3c). Core-to-rim zoning in trace elements is only observed in garnet from Group 3 (plagioclase/scapolite-bearing), where rims show HREE enrichment on primitive mantle normalized spider diagrams ( $Dy_N/Yb_N$  5 – 12, normalized to chondrite) and cores show steep HREE profiles ( $Dy_N/Yb_N$  30 – 155) (Supplemental Figures S5–S6).

**Clinopyroxene:** Core Mg#s and  $Na_2O$  concentrations range from 57 to 78 and 0.78 to 2.9 wt.%, respectively, and do not correlate with lithology (Figs. 3d, 4). All clinopyroxene from garnet-bearing samples shows concave-down trace element profiles on primitive mantle normalized spider diagrams, with pronounced HREE depletion (Supplemental Figures S5–S6). Strong core-to-rim zoning is only observed in clinopyroxenes from sample XC-3–9–16, for which Mg# decreases from 77 to 69 from core to rim.

**Amphibole:** Amphibole in the Mercaderes xenolith suite is calcic, including pargasite and pargasitic hornblende in samples from groups 3–5 and edenite in the diorites (Group 1) (Hawthorne et al., 2012). Core

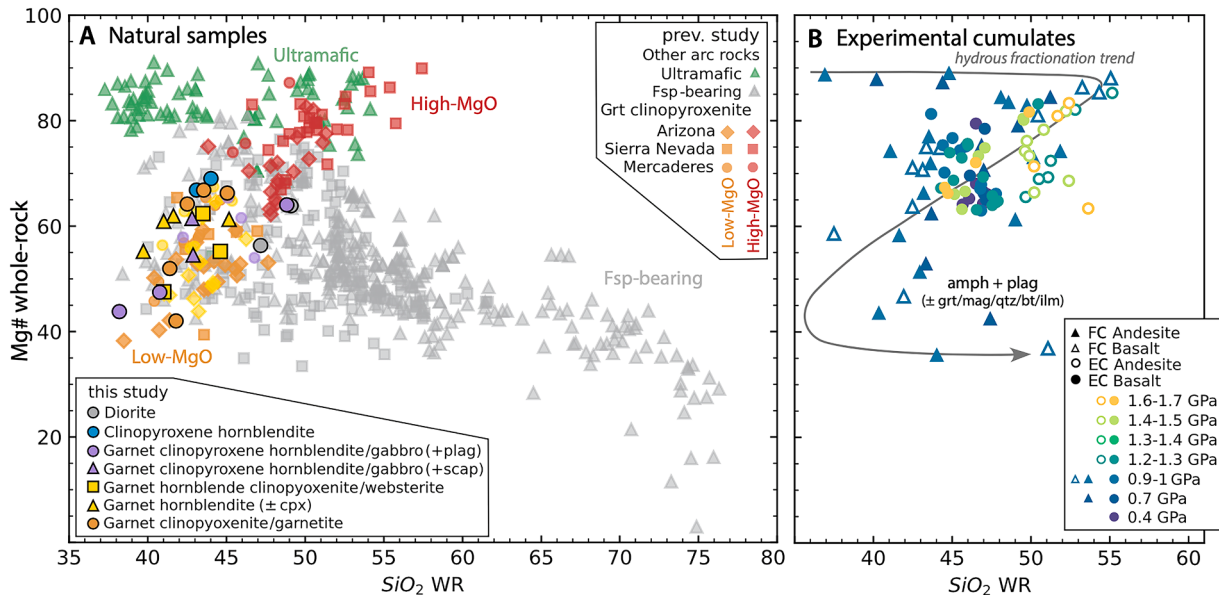


**Fig. 2.** Whole-rock  $SiO_2$  wt.% vs. molar Mg# for (A) natural rocks and (B) experimental cumulates. Previously studied garnet-bearing plutonic xenoliths whole-rock data are from Mercaderes (circles; Weber, 1998; Bloch et al., 2017), Arizona (diamonds; Erdman et al., 2016), Sierra Nevada (squares; Lee et al., 2006). Garnet-free plutonic xenoliths from oceanic and continental arcs are from the Central Aleutians (Sosa et al., 2024) and Lesser Antilles (Cooper et al., 2016). Plutonic whole-rock data from exhumed oceanic and continental arcs include Kohistan (Jagoutz et al., 2006; 2009, 2011), Talkeetna (Greene et al., 2006), and the Sierra Nevada batholith (as compiled in Lewis et al., 2023). Opaque symbols with black borders represent plutonic data from this study, while the literature data are represented by transparent symbols without borders. High and low-MgO garnet clinopyroxenites are classified after Erdman et al. (2016). Hydrous arc fractionation trend is from Müntener and Ulmer (2018) and fractional (FC) and equilibrium (EC) crystallization experimental data are from Villiger et al. (2004, 2007), Alonso Perez (2007), Nandedkar (2014), and Ulmer et al. (2018). Data from Holycross and Cottrell (2023) are omitted because they are not fractional crystallization experiments.

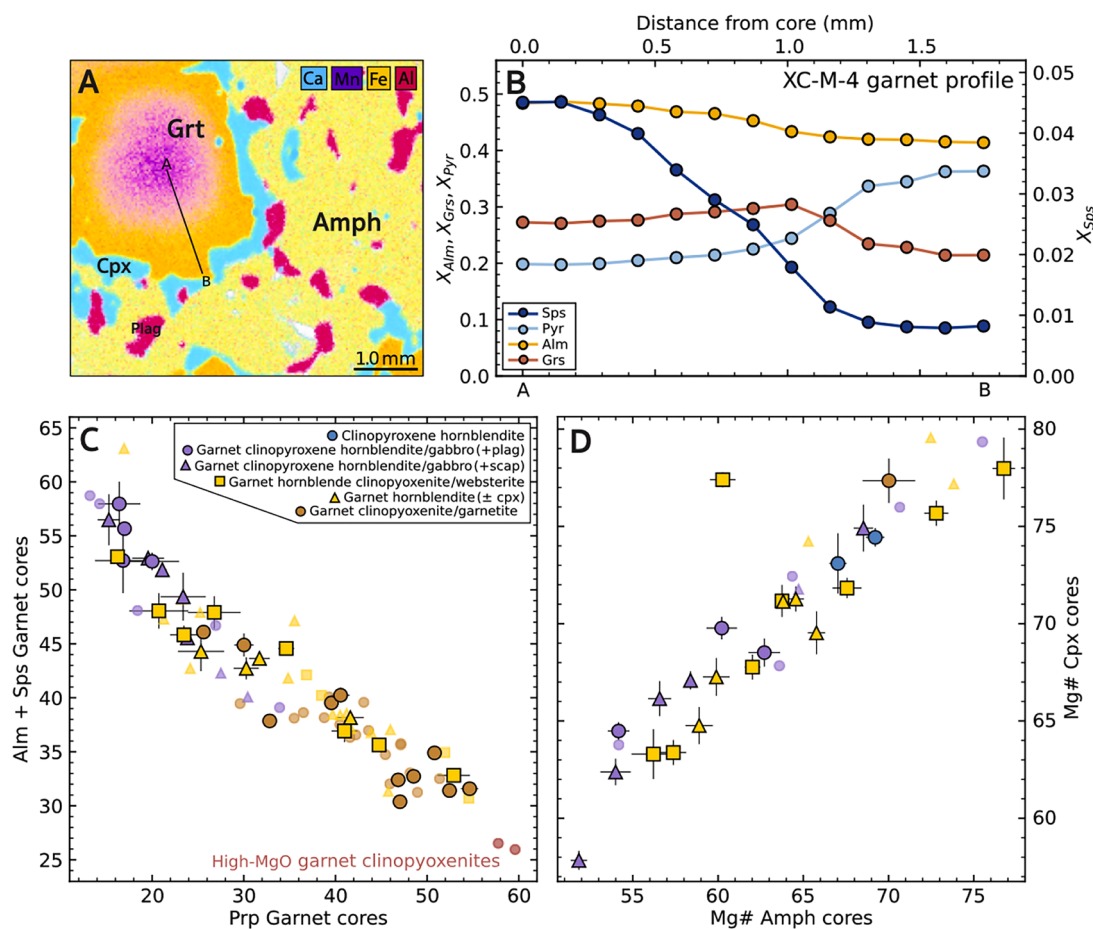


**Fig. 3.** Summary of core mineral chemistry for the Mercaderes xenoliths. **A)** Section of micro-XRF element map of plagioclase-bearing garnet hornblende clinopyroxenite XC-M-4 for Ca, Mn, Fe, and Al. The marked garnet transect corresponds to the EMPA compositional profile in **(B)**, which shows the core-to-rim zoning typical in Mercaderes garnets from compositional Group 3 in terms of spessartite ( $X_{\text{Sps}}$ ), pyrope ( $X_{\text{Pyr}}$ ), almandine ( $X_{\text{AIm}}$ ), and grossular ( $X_{\text{GrS}}$ ) mole fractions. **C)** Average core pyrope content of garnet vs. almandine + spessartite content. **D)** Average core Mg# for amphibole vs. average core Mg# for coexisting clinopyroxene. Literature data (Weber, 1998; Bloch et al., 2017; Zieman et al., 2023; Gianola et al., 2023) are represented by transparent symbols without borders.

amphibole Mg#s range from 51.8 to 76.8 and are generally higher in the plagioclase and scapolite-free assemblages (56.2 – 76.8). Amphibole core Mg# is positively correlated to clinopyroxene core Mg# (Fig. 3d). Trace element concentrations in amphibole are highly variable and do not correlate with Mg# or sample lithology (Supplemental Figures S5-S6). Core-to-rim decreases in Mg# (−0.2 to −7) are seen in 32 % of amphiboles, and core-to-rim increases in Mg# (+0.1 to +2) are present in 56 % of amphiboles, while the remaining 12 % are unzoned.

#### 4.4. Calculated pressures and temperatures

The highest pressures and temperatures are recorded by the garnet clinopyroxenites (1.5–2.2 GPa, 1100–1280 °C), followed by the garnet ( $\pm$  cpx) hornblendites and garnet hornblende clinopyroxenites (generally 1.0–1.9 GPa, 900–1080 °C). Garnet-clinopyroxene geothermobarometry yields a wide array of peak pressure-temperature conditions for the plagioclase and scapolite-bearing hornblendites, ranging from 1.4 to 2.3 GPa and 930 to 1230 °C, with rim compositions generally recording higher pressures and temperatures than the corresponding grain cores (40–500 MPa and 10–150 °C higher). For these amphibole-rich samples, we prefer the pressure-temperature estimates obtained through Perple\_X modeling, ranging from 700 to 975 °C and 0.9–1.5 GPa, as our modeling suggests these compositions would contain high modal proportions of garnet (>50 vol%) at pressures over ~1.2–1.5 GPa. For the clinopyroxene hornblendites, amphibole-only geothermobarometry gives pressure-temperature estimates between

1.6–1.8 GPa and 1010–1050 °C while Perple\_X modeling yields equilibrium conditions between 0.9–1.2 GPa and 700–975 °C. We consider the latter to be more realistic estimates as garnet should stabilize above ~1.3 GPa for these compositions. Amphibole-plagioclase thermometry and barometry for the diorites ( $n = 4$ ) yielded temperature estimates between 650 and 690 °C and pressures from 0.6 to 0.8 GPa. Our preferred pressure-temperature estimate for each sample (and the method employed to obtain that value) is stated in Supplementary Table 9. The geothermal gradient defined by these calculations is consistent with previous studies that have estimated crustal storage conditions with garnet-clinopyroxene geothermobarometry for Mercaderes xenoliths (Bloch et al., 2017; Gianola et al., 2023; Zieman et al., 2023) (Fig. 5a). Density estimates for the xenoliths range from 2.9 to 3.6 g/cm<sup>3</sup> and are highest for garnet clinopyroxenites (3.3 to 3.6 g/cm<sup>3</sup>) and the lowest for diorites (2.9 – 3.0 g/cm<sup>3</sup>).

#### 4.5. Fe isotopes

**Whole-rock:** Whole-rock  $\delta^{56}\text{Fe}$  ranges from −0.02 to 0.11 ‰ and does not correlate with MgO or SiO<sub>2</sub> concentration (Fig. 5b). For the samples where we measured Fe isotope compositions of all modally abundant Fe-bearing phases ( $n = 15$ ), we also calculated theoretical whole-rock  $\delta^{56}\text{Fe}$  values from modal proportions and mineral chemistry. Except for xenoliths XC-MP2-1 and XC-2-09/16, which are coarse-grained and heterogrannular such that modal proportions could not be confidently determined, these calculated whole-rock  $\delta^{56}\text{Fe}$  values are within error

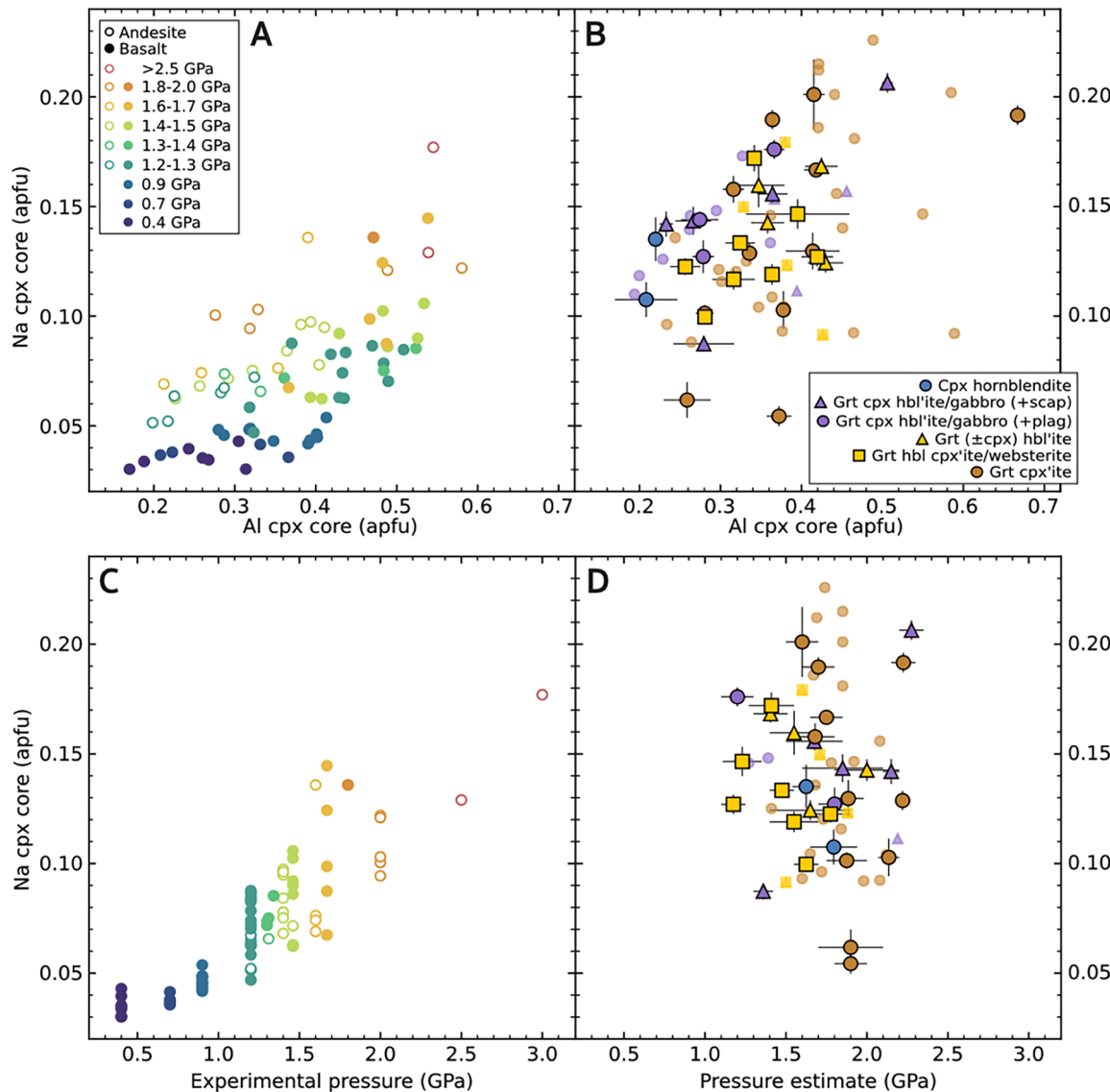


**Fig. 4.** Clinopyroxene compositions from Mercaderes xenoliths compared to clinopyroxenes from experimental studies. Upper panels: clinopyroxene Al vs. Na for experimental studies (Blatter et al., 2013, 2023; Nandedkar et al., 2014; Ulmer et al., 2018; and Holycross and Cottrell, 2023) (A) and Mercaderes xenoliths (B). Lower panels: sample pressure estimate vs. clinopyroxene Na for experimental studies (C) and Mercaderes xenoliths (D). Na and Al are given in atoms per formula unit (apfu). Literature data (Weber et al., 2002; Bloch et al., 2017; Zieman et al., 2023) are represented by transparent symbols without borders in (B) and (D).

(<0.03 ‰) of measured whole-rock compositions (Supplemental Data, Table S15 and Fig. S7).

**Minerals:** Clinopyroxene ( $n = 17$ ,  $\delta^{56}\text{Fe} = +0.08$  to  $+0.23$  ‰) and amphibole ( $n = 10$ ,  $\delta^{56}\text{Fe} = +0.02$  to  $+0.21$  ‰) are the isotopically heaviest phases in all samples, while garnet is the isotopically lightest ( $n = 17$ ,  $\delta^{56}\text{Fe} = -0.17$  to  $+0.03$  ‰) (Fig. 5c). Garnets from the plagioclase and hornblende-bearing rocks (groups 3–5) are the isotopically lightest ( $\delta^{56}\text{Fe} = -0.11$  to  $-0.02$  ‰) while those from garnet clinopyroxenites are slightly heavier ( $\delta^{56}\text{Fe} = -0.05$  to  $+0.02$  ‰). Coexisting clinopyroxene and garnet preserve fractionations ( $\Delta^{56}\text{Fe}_{\text{cpx-grt}}$ ) of  $+0.07$  to  $+0.33$  ‰ (Supplemental Figure S8). In general, the garnet clinopyroxenites are characterized by lower  $\Delta^{56}\text{Fe}_{\text{cpx-grt}}$  ( $+0.07$  to  $+0.19$  ‰) than the hornblendites ( $\pm$  scapolite/plagioclase) ( $+0.17$  to  $+0.33$  ‰). Inter-mineral isotopic fractionation between coexisting amphibole and garnet ranges from  $\Delta^{56}\text{Fe}_{\text{amph-grt}} = +0.17$  to  $+0.30$  ‰ and is higher in hornblendite ( $\pm$  scapolite/plagioclase) xenoliths ( $\Delta^{56}\text{Fe}_{\text{amph-grt}} = +0.23$  to  $+0.30$  ‰) compared to clinopyroxenites ( $\Delta^{56}\text{Fe}_{\text{amph-grt}} = +0.17$  to  $+0.23$  ‰) (Supplemental Figure S8). Coexisting clinopyroxene and amphibole in the Mercaderes xenoliths show markedly less inter-mineral isotopic

fractionation, with  $\Delta^{56}\text{Fe}_{\text{cpx-amph}}$  ranging from  $-0.03$  to  $+0.07$  ‰ (Supplemental Figure S8).

**Force constant estimates:** Consistent with our data, previous studies of Fe isotopes in igneous and metamorphic rocks have found amphibole and clinopyroxene to be isotopically heavier than coexisting garnet ( $\Delta^{56}\text{Fe}_{\text{cpx-grt}}$  and  $\Delta^{56}\text{Fe}_{\text{amph-grt}}$   $+0.1$  to  $+0.5$  ‰; Beard and Johnson, 2004; Williams et al., 2005; Dauphas et al., 2009; Li et al., 2016; Liang et al., 2022), suggesting the amphibole and clinopyroxene force constants should both be significantly higher than that of garnet ( $<\!F>_{\text{almandine}} = 110 \text{ N/m}$ ; Nie et al., 2021). We can estimate appropriate force constants for clinopyroxene and amphibole from our Fe isotope data and temperature estimates for each sample. These calculations were performed using the relationship between the permil fractionation ( $\Delta$ ) and force constants of two phases (A and B) at equilibrium at a given temperature for each sample (Dauphas et al., 2014):

$$\Delta^{56}\text{Fe}_{B-A} = \delta^{56}\text{Fe}_B - \delta^{56}\text{Fe}_A = 2853[\langle F \rangle_B - \langle F \rangle_A]/T^2 \quad (2)$$

Given the sensitivity of these calculations to changes in temperature, thermobarometry and Perple\_X modeling were rigorously interrogated

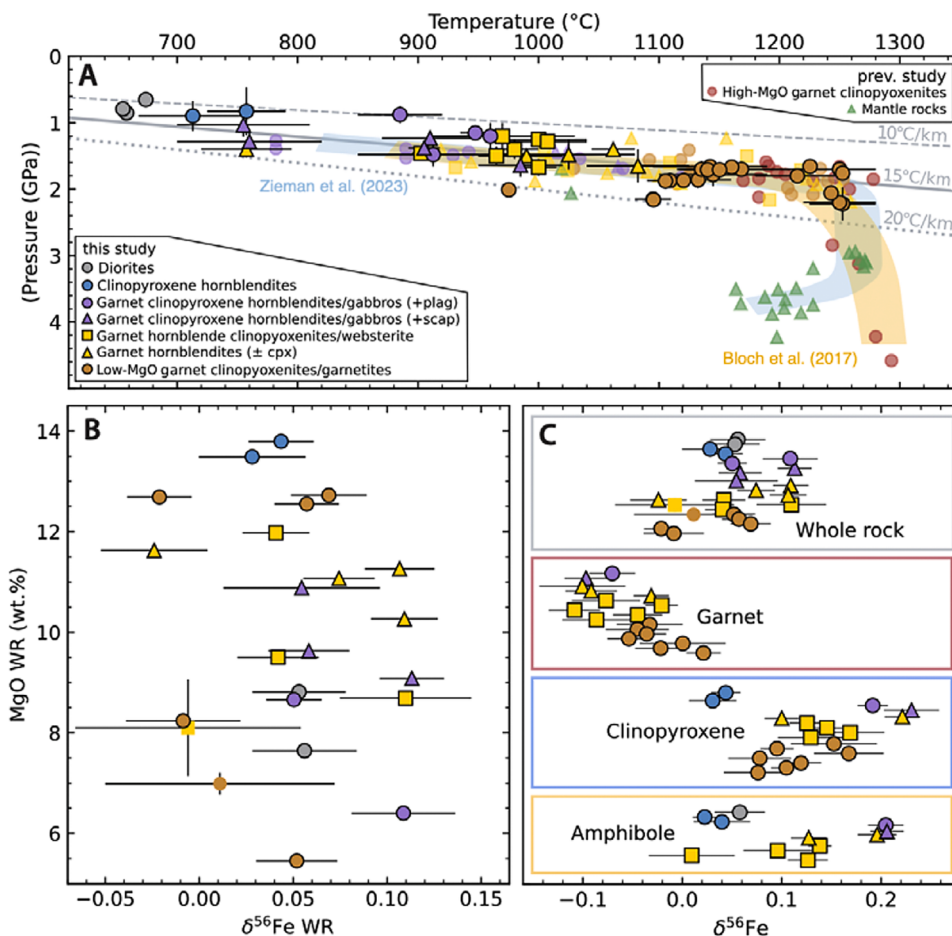


**Fig. 5.** Fe isotope data and pressure/temperature estimates for Mercaderes xenoliths. A) Maximum  $P$ - $T$  estimates for Mercaderes xenoliths. Literature data (Bloch et al., 2017; Zieman et al., 2023) are represented in opaque symbols. For pressure-temperature estimates obtained through garnet-clinopyroxene or amphibole-plagioclase geothermobarometry, error bars represent the range obtained by simultaneously solving the geothermometer and barometer while varying mineral compositions for each sample (see the Supplemental Data for details). Geotherm gradients are calculated assuming a 35 km per GPa pressure-to-depth conversion. B) Whole-rock  $\delta^{56}\text{Fe}$  vs. MgO. C) From top to bottom panel, Fe isotope data for whole-rock powders, garnet, clinopyroxene, and amphibole from Mercaderes samples, organized by lithological groups. The greatest  $\Delta^{56}\text{Fe}_{\text{cpx-grt}}$  and  $\Delta^{56}\text{Fe}_{\text{amph-grt}}$  are observed in the lower-temperature Group 3 samples (grt + cpx + amph + plag/scap), while the least inter-mineral Fe isotope fractionation is seen in the Group 6 samples (grt + cpx). Symbols without black borders in (B) and (C) represent whole-rock compositions calculated from mineral chemistry, modes, and densities.

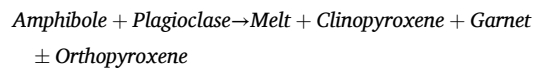
for each sample used in estimating  $\langle F \rangle_{\text{amph}}$  or  $\langle F \rangle_{\text{cpx}}$  (Supplemental Figures S1–2). We calculated weighted average values of  $\langle F \rangle_{\text{cpx}} = 227 \pm 17 \text{ N/m}$  and  $\langle F \rangle_{\text{amph}} = 232 \pm 21 \text{ N/m}$ , with errors derived from temperature uncertainties for each sample. There is no systematic difference in calculated  $\langle F \rangle_{\text{amph}}$  or  $\langle F \rangle_{\text{cpx}}$  for each sample based on lithology or equilibrium temperature, suggesting that the observed increase in inter-mineral isotopic fractionation ( $\Delta^{56}\text{Fe}_{\text{cpx-grt}}$  and  $\Delta^{56}\text{Fe}_{\text{amph-grt}}$ ) in the hornblendite xenoliths reflect lower equilibrium temperatures for these samples and that our temperature estimates are associated with Fe isotope equilibrium (Supplemental Figure S10).

## 5. Discussion

### 5.1. Textural and chemical evidence for restitic garnet clinopyroxenite origins

The textural and mineralogical variations observed in the Mercaderes xenoliths are consistent with previous conclusions that the Mercaderes xenoliths preserve an amphibolite to granulite facies transition in the lower crust, with amphibole-dehydration melting leading to the formation of garnet clinopyroxenite residues (Weber et al., 2002; Giannola et al., 2023). The transition from amphibole and plagioclase-dominated lithologies (groups 1 and 2: diorites and

clinopyroxene-hornblendites) to those dominated by clinopyroxene and garnet is marked by strongly zoned porphyroblastic garnet with coronae of clinopyroxene in a matrix of amphibole and plagioclase (Group 3: Fig. 3a), suggesting incomplete transformation and equilibration to a garnet clinopyroxenite assemblage. Common features of retrograde metamorphism, such as plagioclase + clinopyroxene or plagioclase + amphibole symplectites/coronae around garnet (Zhao et al., 2001), are not observed in the Mercaderes xenoliths, consistent with a prograde metamorphic origin. Most garnets from the transitional metamorphic assemblages (groups 3–5) also show core-to-rim decreases in MnO and HREEs and increases in MgO, characteristic zoning patterns of prograde metamorphic garnet (e.g., Spear and Selverstone, 1983; Rubatto et al., 2020). These textural observations are consistent with amphibole dehydration reactions involving the consumption of amphibole and plagioclase:



In addition, other geochemical characteristics of the Mercaderes xenoliths are inconsistent with a cumulate origin, such as the lack of correlation between major/trace element data and lithology or modal assemblage (for both whole-rock and mineral analyses). For example,

experimental studies show that with increased pressure, clinopyroxene in equilibrium with melt (during both fractional crystallization or partial melting events) develops a greater jadeite component, increasing Al and Na concentrations (e.g., Blundy et al., 1995). Clinopyroxenes from equilibrium crystallization experiments, therefore, show strong positive correlations between Al, Na, and pressure (Fig. 4). No correlations are observed, however, between Al and Na composition in clinopyroxenes or Al and Na as a function of calculated pressure (Fig. 4). These data can be explained if clinopyroxene Al and Na content in the garnet-bearing rocks (groups 3–6) is not reflective of equilibrium between melt and clinopyroxene during partial melting, but rather controlled, in part, by the composition of their diorite protoliths. Indeed, at a given pressure and Al content, the Na contents of the Mercaderes clinopyroxenes are higher than that in the experimental data, suggesting Na inheritance from plagioclase±amphibole in their protoliths.

These lines of evidence are consistent with the following model, in which garnet-free diorites (Group 1) and clinopyroxene hornblendites (Group 2) represent the least metamorphosed starting compositions, and garnet-bearing gabbros, hornblendites, and clinopyroxenites (groups 3 to 5) represent transitional (disequilibrium) metamorphic assemblages. Within this framework, the garnet clinopyroxenite and garnetite xenoliths (Group 6) represent the full consumption of amphibole rather than cumulates from basalt crystallization. Previous documentation of high silica melt inclusions in garnet (65.3–72.4 wt.% SiO<sub>2</sub>; Gianola et al., 2021) from Mercaderes xenoliths is consistent with this model and is strong evidence that the host minerals grew in the presence of a felsic melt, likely generated through amphibole dehydration reactions. We note that while previous studies have shown that amphibole ± plagioclase assemblages may form via peritectic reaction of garnet + pyroxene with dacitic to rhyolitic liquids at ~1 GPa (e.g., Blatter et al., 2023), we consider it unlikely that this would be a dominant process for the formation of the Mercaderes suite, as it would imply a significant quantity of relatively viscous silicic melt of unknown origin percolating upward from deeper in the lower crust. We now turn to the Fe isotope data, which adds a new dimension of support to this argument, as well as the implications of our findings for the Fe isotopic evolution of arc magmas and the composition of the Andean crust.

## 5.2. Fe isotopes

A first-order observation of the Mercaderes dataset is that there is little variability in the whole-rock Fe isotope composition of the Mercaderes suite across all lithologies (average whole-rock  $\delta^{56}\text{Fe} = 0.06 \pm 0.04$ ), suggesting that the process responsible for the formation of the suite resulted in limited Fe isotope fractionation. We explore the two competing models of garnet clinopyroxenite formation via 1) crystal accumulation from a melt or 2) as restitic products from amphibole dehydration. The predicted behavior of Fe in these systems is dramatically different. To conceptually illustrate this, we briefly examine the behavior of Fe in crystallization and partial melting experiments relevant to these two models. Blatter et al. (2023) show a primitive arc basalt with ~9.5 wt.% FeO crystallizing at ~1.7 GPa saturates with clinopyroxene (and minor orthopyroxene) at ~1250 °C, followed shortly by garnet at ~1200 °C. By 1150 °C, ~40 % of the initial magma has crystallized, and FeO in the melt begins to drop precipitously due to the onset of garnet crystallization, with ~80 % of the melt's initial Fe incorporated into cumulate minerals by 1050 °C.

In contrast, for a dehydration melting scenario, melt production is much more limited because it is constrained by the amount of amphibole in the protolith available to break down. Mafic amphibolite partial melting experiments conducted at 1.5–2 GPa and 850–1150 °C by Sen and Dunn (1994) chronicle the transformation of amphibole and plagioclase-dominated assemblages to garnet clinopyroxenites. As melt was produced, the whole-rock Mg# of the residue increased from 53 to 69, similar to what is observed between the Mercaderes diorites and garnet clinopyroxenites (Mg# increases from 56 to 67). These

experiments generated a maximum of ~25 % melting, with only 14 % of the initial Fe of the protolith lost to the liquid. Conceptually, although isotopic fractionations will be large at low temperatures during amphibole dehydration melting, mass balance dictates that the Fe isotopic composition of the residue should not be significantly affected due to the small volumes of Fe-poor melt being extracted. Therefore, progressive metamorphism of dioritic protoliths should produce a suite of residues with relatively unfractionated Fe isotope compositions, similar to what is observed in our whole-rock measurements of the Mercaderes xenoliths.

We quantitatively explore whether the Fe isotope data is consistent with formation through crystallization from a melt (Model A; Fig. 6) versus metamorphic dehydration reactions (Model B; Fig. 7) by modeling the Fe isotope trajectories expected for each process. The most salient features of these models are discussed below, while greater details of model parameters, justification of starting compositions, and additional results are given in the Supplemental Data.

*Fractional crystallization (Model A):* We first construct a model to explore the evolution of primitive arc basalts undergoing fractional crystallization as they ascend through thickened arc crust using Perple\_X. We start with a representative primitive Colombian basalt (Supplemental Figure S11) with 3 wt.% H<sub>2</sub>O at an initial oxygen fugacity of FMQ+1 and fractionally crystallize the melt along the Mercaderes geothermal gradient (~1300 °C, 2 GPa to 800 °C, 1 GPa). While we prefer the parameters chosen in this model as they most accurately reproduce the observed mineralogy of the Mercaderes suite, sensitivity tests exploring the effect of variable water content (2–6 wt.%), major element composition (Mg-andesites to Mg-basalt), and initial oxygen fugacity (FMQ to FMQ+2) are given in the Supplemental Data (Supplemental Figures S13–S14). In our model, clinopyroxene enters as a liquidus phase at 1285 °C followed by garnet at 1210 °C. During garnet clinopyroxenite fractionation, 55–80 % of the Fe in the crystallizing cumulate for each step is sequestered by garnet (Fig. 6a, b). After ~50 % garnet clinopyroxenite fractionation, amphibole saturates at 940 °C, becoming the dominant Fe-bearing phase in the cumulate assemblage, clinopyroxene crystallization ceases, and garnet modal abundances decrease rapidly. Plagioclase does not saturate until 840 °C.

From these major element and modal constraints, we constructed a simple mass balance model to constrain the Fe isotope evolution of both the melt and cumulate during fractional crystallization:

$$\delta^{56}\text{Fe}^{i+1}_{\text{melt}} = \delta^{56}\text{Fe}^i_{\text{melt}} + \Delta^{56}\text{Fe}_{\text{melt-cumulate}}^{i+1} (1 - f^{i+1}) \quad (3)$$

where  $f$  is the fraction of Fe in the melt relative to the system at each fractionation step,  $i$ . As we have no isotopic constraints for primary Andean basalts, we use an initial  $\delta^{56}\text{Fe}$  of 0.0 ‰. Our model shows that garnet clinopyroxenite crystallization should result in significant cumulate-melt fractionation ( $\Delta^{56}\text{Fe}_{\text{melt-cumulate}} = +0.07$  to  $+0.17$  ‰) and an early interval of isotopically light cumulate production (Fig. 6c). Continued removal of isotopically light Fe from garnet crystallization drives more evolved melts to heavier  $\delta^{56}\text{Fe}$  compositions, with >60 % of the initial Fe in the system lost to garnet fractionation between ~1200 and 800 °C (Fig. 6b).

Our model results suggest garnet clinopyroxenite fractionation should produce an isotopically light lower crust and an isotopically heavy amphibole-bearing middle to upper crust. Such isotopic stratification of arc crust has been observed in cumulate xenoliths from the oceanic Central Aleutian Arc, where olivine-rich dunites create an isotopically light lower-crustal reservoir relative to amphibole and magnetite-rich mid-crustal gabbros (Sosa et al., 2024), findings differing significantly from the relatively uniform isotopic compositions observed in the Mercaderes xenoliths (whole-rock  $\delta^{56}\text{Fe} = -0.02$  to  $+0.11$  ‰, with 86 % of all samples between  $+0.03$  ‰ and  $+0.11$  ‰.). This model, and all performed sensitivity tests, are also inconsistent with the Fe isotope trends observed in minerals separated from Mercaderes rocks (Fig. 6d; Supplemental Figure S13).

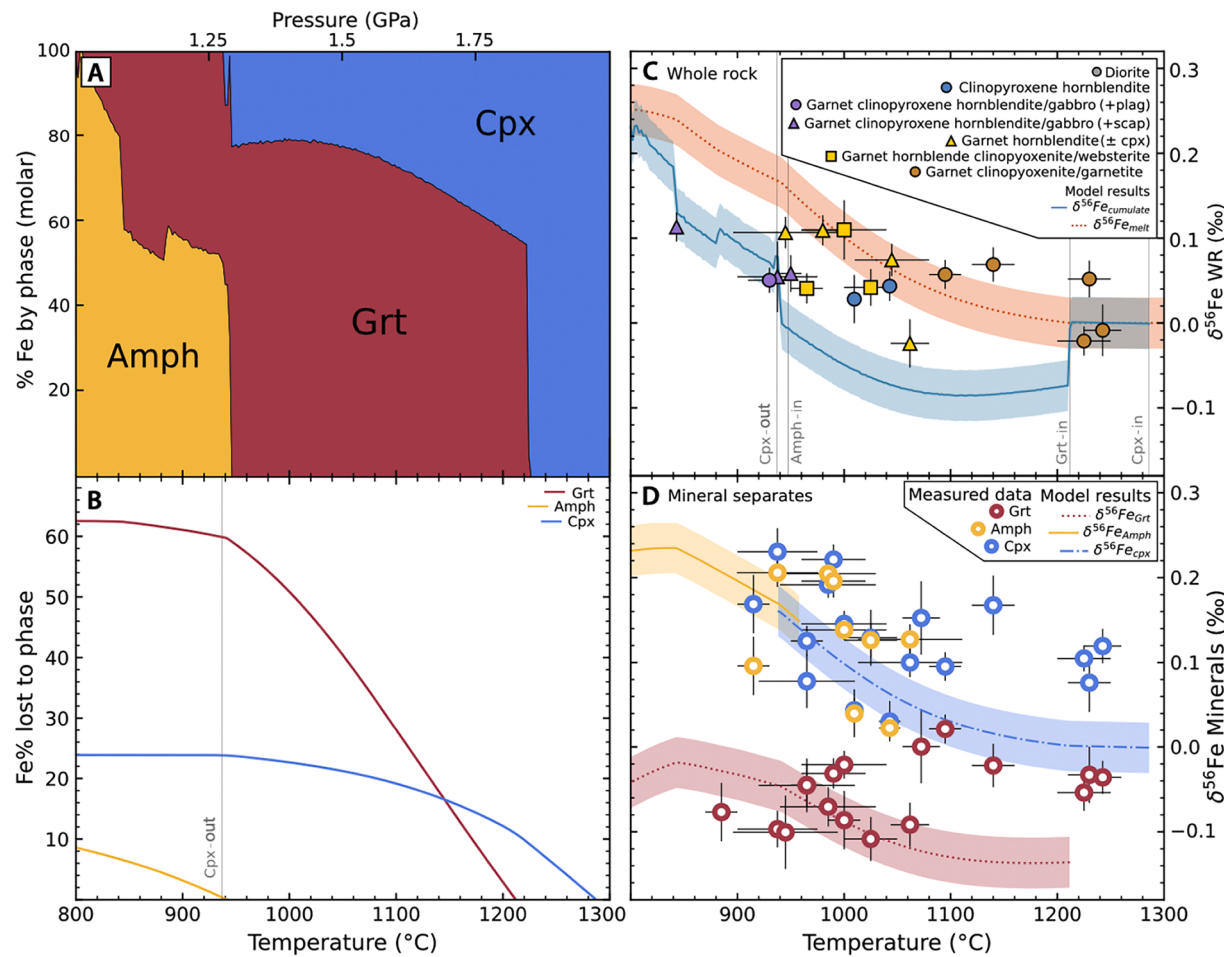


**Fig. 6.** Fractional crystallization Fe isotope model results. **A)** Distribution of Fe between coexisting clinopyroxene, garnet, and amphibole in instantaneous fractionated cumulate. **B)** Cumulative percentage of initial Fe in the melt removed through fractionation of each phase in the model. **C)** Isotopic evolution of a basaltic melt with an initial  $\delta^{56}\text{Fe}$  of 0.0‰ (dotted line) and Fe isotope composition of the complementary instantaneous cumulate (solid line). **D)** Model results for Fe isotope composition coexisting of amphibole (solid line), clinopyroxene (dot-dashed line), and garnet (dotted line) in cumulate compared to measured mineral separates. Shaded transparent fields represent 0.03‰ variability in  $\delta^{56}\text{Fe}$  in (C) and (D).

**Amphibole dehydration melting (Model B):** We now turn to the hypothesis that the Mercaderes xenolith suite may instead represent a prograde metamorphic sequence. Using Perple\_X and a representative diorite whole-rock composition (sample XC-MG-5), we constructed a model in which our protolith is brought to higher pressure and temperatures along the Mercaderes geothermal gradient (Fig. 7a). We use an initial  $\text{Fe}^{+3}/\Sigma\text{Fe} = 0.30$  and water content of 1.2 wt.%, which we consider an appropriate estimate for a diorite protolith containing ~60 % amphibole with ~2 wt.% structurally bound water.

The melts generated in this model should not segregate from the protolith until interconnected channels are established within the residue. Estimates of the necessary melt volume required to attain channelization vary from 2 to 10 wt.% (e.g., Wolf and Wyllie, 1991; Vigneresse et al., 1996), and we chose 7 wt.% as a reasonable estimate (same value used by Bowman et al., 2021). Assuming incomplete melt segregation during extraction (e.g., Sawyer, 2014), we leave 0.5 wt.% melt in the residue after each extraction event. Sensitivity tests were also performed for this model, in which we varied water content (0.5–1.5 wt.% H<sub>2</sub>O), diorite composition, initial  $\text{Fe}^{+3}/\Sigma\text{Fe}$  (0.15–0.30), the threshold at which melt is extracted (4–10 wt.% melt),  $\langle F \rangle_{\text{amph}}$  (211–253 N/m),  $\langle F \rangle_{\text{cpx}}$  (210–244 N/m), and the amount of melt left in the residue after each extraction event (0.1–1.0 wt.% melt) (Supplemental Figure S15).

We use an initial Fe isotope composition of  $\delta^{56}\text{Fe} = +0.06\text{ ‰}$  (average diorite value). Amphibole dehydration melting begins at 806 °C (Fig. 7b), with amphibole exhausted from the residue by 1094 °C

after ~27 wt.% melt extraction. Plagioclase is fully consumed by 1124 °C (Fig. 8b). At 2 GPa and 1300 °C, the residue is composed completely of garnet and clinopyroxene with  $\delta^{56}\text{Fe} = 0.03\text{ ‰}$  (Fig. 7c), and a total of 35 wt.% melt has been extracted. The relatively uniform  $\delta^{56}\text{Fe}$  of the modeled residue from 800 to 1300 °C is consistent with most measured Mercaderes xenoliths (Fig. 7c). Our model is also consistent with the observed trends in amphibole, garnet, and clinopyroxene Fe isotope chemistry (Fig. 7d). The residue experiences little isotopic change because the melts generated are Fe-poor below ~1100 °C ( $1\text{--}6\text{ ‰ Fe}_{\text{OT}}$ ) and most of the Fe remains in the solid, with  $\text{Fe}_{\text{OT}}$  in the residue increasing from 10.6 wt.% at 800 °C to 13.5 wt.% at 1300 °C (normalized anhydrous). These results imply that the Andean crust in the Mercaderes region has a near-constant Fe isotope composition from ~2 to ~0.6 GPa (~70 to 21 km below the surface, assuming a pressure-to-depth conversion of 35 km/GPa), contrary to the expectation that garnet fractionation should create an isotopically light lower crust if crystallizing from a typical mantle melt.

The dramatic difference in the isotopic evolution of modeled cumulates and residues arises from the contrasting behavior of Fe in each system. Between 1300 and 800 °C, 75 % of the initial melt in the system crystallizes and 95 % of the initial Fe is consumed by cumulates in Model A (Fig. 8c). In contrast, because the melts formed in the amphibole dehydration model are generally Fe-poor andesites below 1125 °C, when the majority (28 wt.%) of melt generation occurs, only 21 % of the initial Fe in the system is lost to the melt between 1300 and 800 °C in

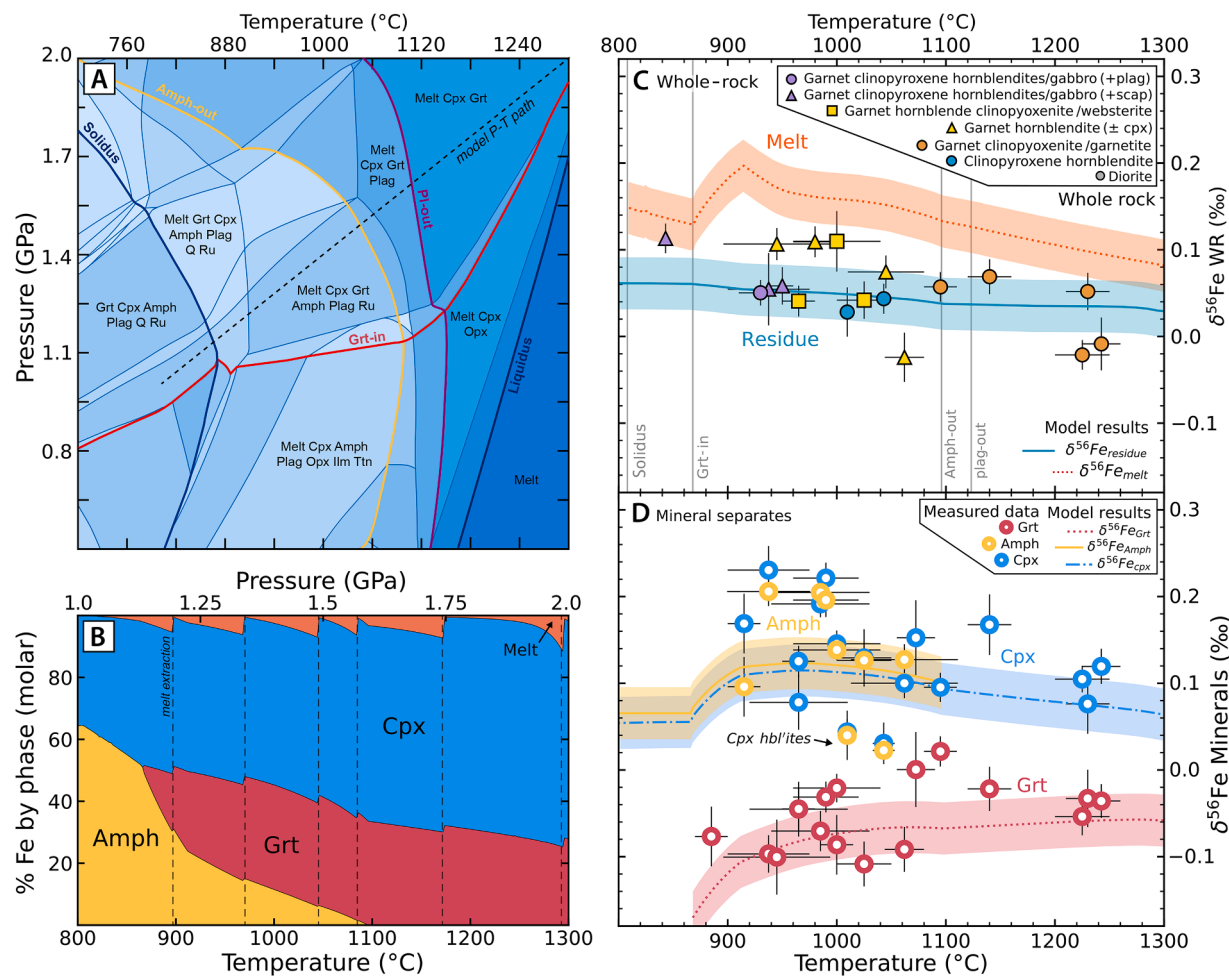


**Fig. 7.** Amphibole dehydration partial melting Fe isotope model results. **A)** Perple\_X pseudosection made with the whole-rock composition of diorite XC-MG-5, assuming initial  $\text{Fe}^{+3}/\Sigma\text{Fe}$  of 0.3 and 1.2 wt.%  $\text{H}_2\text{O}$ . The dashed line in (A) represents the metamorphic path followed in (B), (C), and (D). **B)** Distribution of Fe between coexisting melt, clinopyroxene, garnet, and amphibole during prograde metamorphism. Dashed vertical lines represent melt extraction events. **C)** Fe isotope evolution of metamorphic residue (solid line) and complementary partial melts (dotted line) assuming an initial  $\delta^{156}\text{Fe}$  of +0.06‰. Measured whole-rock Fe isotope compositions and temperature estimates for Mercaderes xenoliths are shown for comparison. **D)** Model results for Fe isotope composition of coexisting amphibole (solid line), clinopyroxene (dot-dashed line), and garnet (dotted line) in residue compared to measured mineral separates. Shaded transparent fields represent 0.03‰ variability in  $\delta^{156}\text{Fe}$  in (C) and (D).

Model B (Fig. 8d). The modal dominance of garnet in the crystallizing cumulates between 1210 and 940 °C in Model A also results in greater melt-solid isotopic fractionation ( $\Delta^{156}\text{Fe}_{\text{melt-cumulate}} = +0.07$  to +0.17 ‰) (Fig. 8e, g) compared to amphibole dehydration melting in Model B over the same temperature range ( $\Delta^{156}\text{Fe}_{\text{melt-residue}} = +0.07$  to +0.12 ‰) (Fig. 8f, h).

### 5.3. Implications for crustal structure and evolution

The possibility of lower to mid-crustal gabbros (or basalts) undergoing densification reactions in response to orogeny and burial, and the importance of such phase transitions in promoting lower-crustal delamination, has been long recognized (e.g., Kay and Kay, 1991, 1993; Wyllie and Wolf, 1993; Jull and Kelemen, 2001). Eclogite formation may create inverted density gradients and gravitational instabilities at the crust-mantle interface that promote lower-crustal delamination, either through “peeling” (i.e., separation of dense garnet clinopyroxenite roots at a laterally propagating rift: Bird, 1979) or as “drips” (i.e., discrete packages of dense root material falling from the crustal base: Jull and Kelemen, 2001). Evidence of recent delamination has been observed and extensively studied further south in the Andean belt, where rising asthenospheric mantle has resulted in rapid tectonic

uplift, changes in regional stress regime, and abrupt shifts from felsic to mafic volcanism (e.g., Mpodozis and Kay, 1992; Kay et al., 1994). Debate exists, however, as to whether metamorphism of gabbroic assemblages or crystallization of garnet clinopyroxenite cumulates provides the impetus for delamination, as it has been argued that gabbro densification is an inefficient means of generating dense mafic residues (e.g., Saleeby et al., 2003).

While our Fe isotope data favor the formation of low-MgO garnet clinopyroxenites through metamorphism, they do not have any bearing on the origin of high-MgO garnet clinopyroxenites, which have been described in previous studies of Mercaderes xenoliths (Rodríguez-Vargas et al., 2005; Bloch et al., 2017; Zieman et al., 2023; 2024) but were not present in our sample suite. Our data, therefore, do not discredit nor support the existence of cumulates at the very base of the Andean crust or upper-most mantle, which awaits further study. While trace elements systematics of erupted lavas from the Andean NVZ show clear signs of garnet equilibration (e.g., Bryant et al., 2006), which could reflect a prolonged period of deep garnet fractionation, these signatures could also be created by mixing between mantle-derived magmas and partial melts generated by amphibole dehydration reactions, which would also be in equilibrium with garnet. Indeed,  $\delta^{156}\text{Fe}$  values of the (basaltic) andesites and dacites generated in our amphibole dehydration model

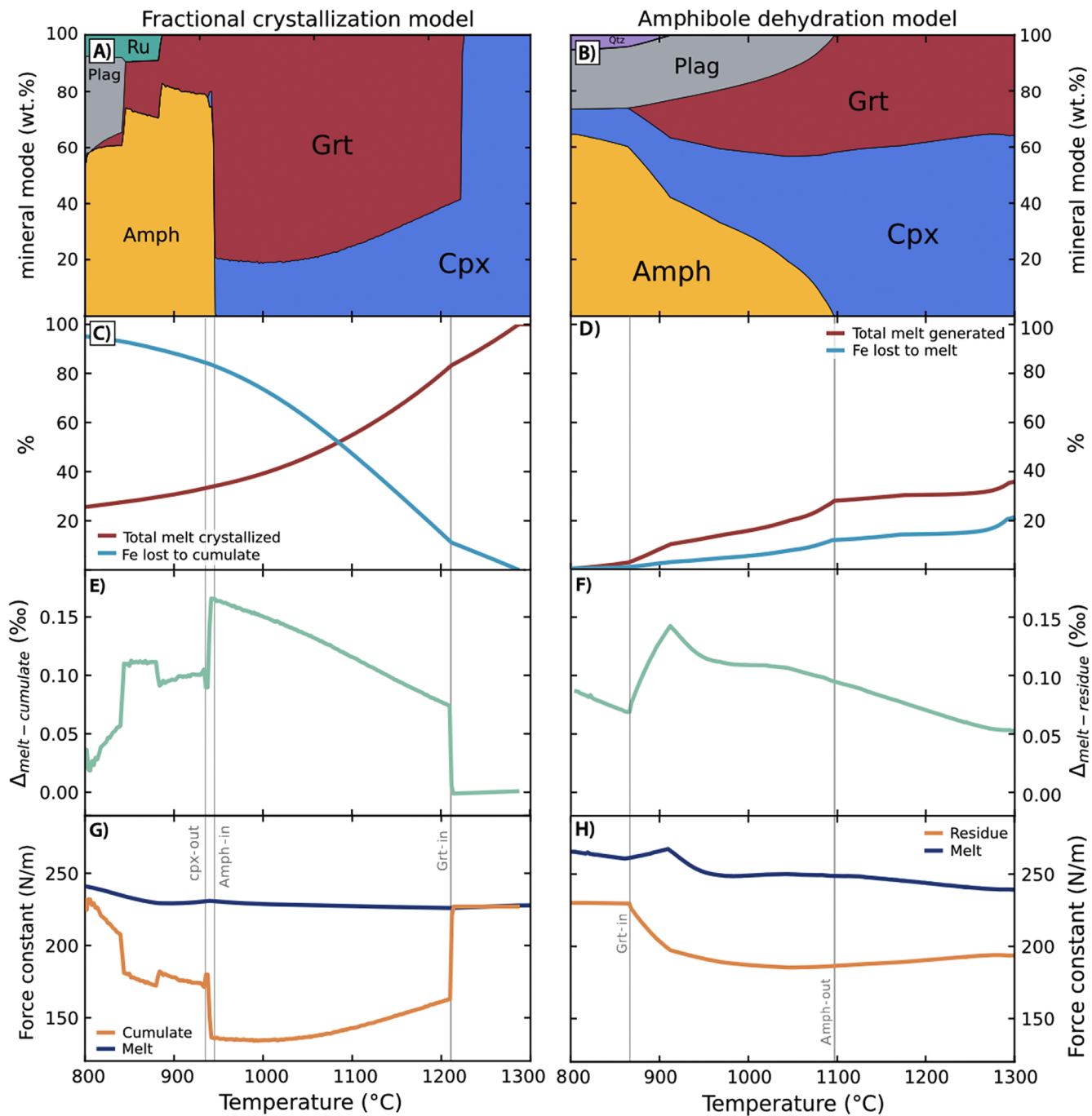


**Fig. 8.** Comparison between fractional crystallization and amphibole dehydration models. **A)** instantaneous modal mineral abundances (wt.%) of fractionated cumulate. **B)** Modal abundance of coexisting phases in the metamorphic residue of the amphibole dehydration model. The increased isotopic fractionation between the melt and solid for the two models is also shown in plots of  $\langle F \rangle_{\text{melt}}$  vs.  $\langle F \rangle_{\text{solid}}$  and  $\Delta^{56}\text{Fe}_{\text{melt-cumulate}}$  for the fractional crystallization (**C, E**) and amphibole dehydration (**D, F**) models. **G)** Total amount of melt crystallized and percentage of initial Fe lost to the fractionating cumulate. **H)** Total melt generated and percentage of initial Fe from the diorite protolith lost to the melt in the amphibole dehydration model.

range from +0.08 to +0.20 ‰, similar to previous studies of Andean (basaltic/trachy-) andesite and dacites from over-thickened (>45 km) regions of the Central Volcanic Zone further south ( $\delta^{56}\text{Fe} = +0.12$  to +0.19 ‰ Du et al., 2023).

A possible scenario for the formation of the Mercaderes crust might, therefore, be a hybrid of the gabbro-metamorphism and cumulate models: primitive basalts may (or may not) fractionate high-MgO garnet clinopyroxenites at the base of the Andean crust before ascending to shallow crustal levels, where they fractionate diorites at pressures below the garnet stability field. Crustal thickening in response to orogeny or

burial under the growing cumulate pile may bring these rocks to greater depths, driving amphibole dehydration melting of original diorite cumulates, forming garnet clinopyroxenites (Fig. 9). In conjunction with the densification of high-MgO garnet clinopyroxenite roots, amphibole dehydration may, therefore, also drive delamination of the lower Andean crust. At the pressures and temperatures specified by geothermobarometry and Perple\_X modeling, calculated densities for the diorites and garnet clinopyroxenites range from 2.9 to 3.0 g/cm<sup>3</sup> and 3.4 to 3.6 g/cm<sup>3</sup>, respectively, implying that the latter would be gravitationally unstable relative to the mantle (~3.3–3.4 g/cm<sup>3</sup>). This

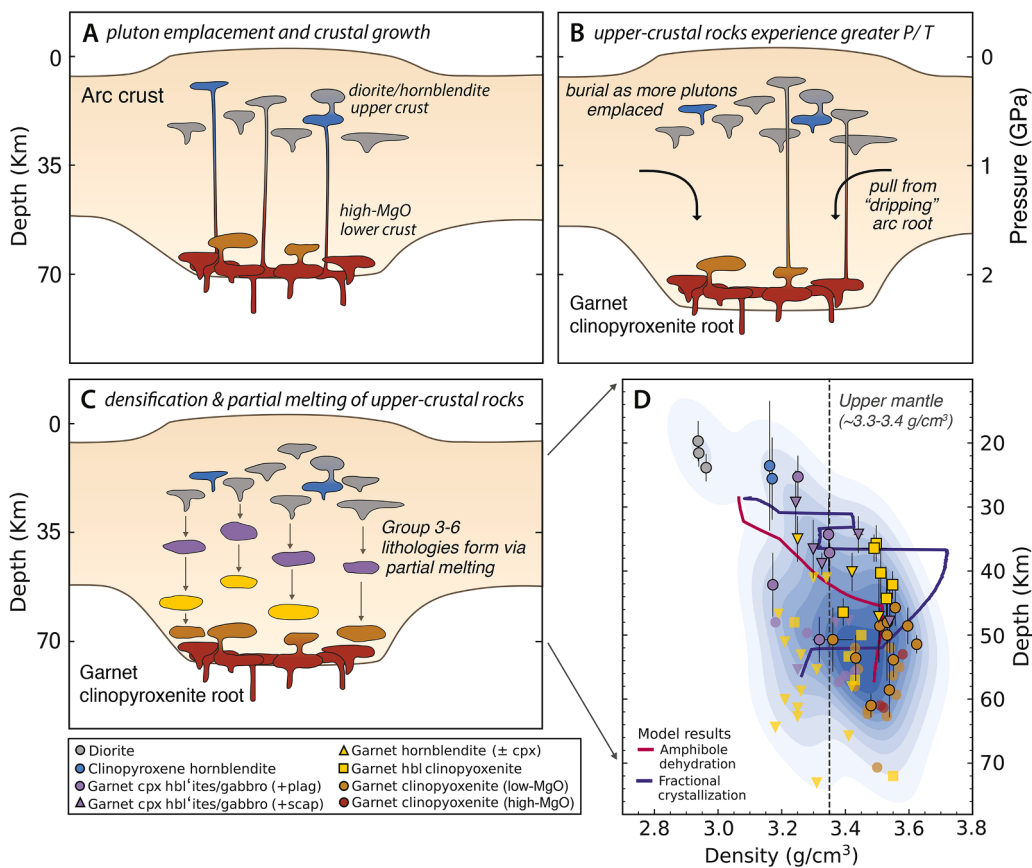


**Fig. 9.** Schematic illustration of crustal formation (A-C) and density structure (D) of the Mercaderes crust. **A)** Initial emplacement of diorite and hornblendite protoliths. High-MgO lower crustal root is shown but we do not speculate on its origin. **B)** Upper-crustal plutons experience greater pressures and a downward “pull” in response to 1) burial as more plutons are emplaced above and 2) the downward pull of dense garnet clinopyroxenite roots as they begin to delaminate in a “lithospheric-drip” type model. **C)** Upper-crustal plutons undergo amphibole dehydration (i.e., densification) reactions in response to increased pressure and temperature, resulting in the formation of garnet-bearing residues (i.e., compositional groups 3–6). **D)** Density structure of the Mercaderes crust inferred from geothermobarometry and Perple\_X modeling using a 35 km/GPa pressure-to-depth conversion. Xenolith densities were calculated using the meemum Perple\_X function. Densities of solids in fractional crystallization and partial melting models are also shown for context, with both resulting in the formation of garnet clinopyroxenite roots that are gravitationally unstable relative to the underlying mantle (~3.3–3.4 g/cm<sup>3</sup>). Literature density calculations for Mercaderes xenoliths (including low and high-MgO samples) represented by transparent symbols are from Zieman et al. (2023).

densification is reflected in our Perple\_X amphibole dehydration model, where metamorphism is associated with increased residue density from 3.0 to 3.5 g/cm<sup>3</sup> (Fig. 9d).

Recent studies have interpreted the chemistry of low-MgO garnet clinopyroxenites as representative of magmatic conditions (e.g., Tang et al., 2018), but this must be done cautiously. Iron isotopes offer a powerful tool to disentangle the effects of garnet crystallization vs. gabbro/diorite metamorphism, but should be integrated with robust petrographic and major/trace element characterization. While our results do not preclude the importance of deep garnet fractionation in generating the light Fe isotope compositions and HREE observed in lavas from thickened arc sections, they do suggest that amphibole dehydration reactions may represent an important, previously overlooked source of these signatures. Future work on Fe isotopes in high-MgO garnet clinopyroxenites from continental arcs is clearly warranted, as our dataset does not cover the full compositional diversity seen in these suites. Critically, our new Fe isotope data from the Mercaderes suite support previous studies that have suggested that gabbro densification has played an important role in the development of the lower Andean crust (e.g., Kay and Kay, 1991, 1993; Weber et al., 2002). This means that not all garnet clinopyroxenites suites will display light Fe isotope signatures because they are not all formed through lower-crustal crystallization-differentiation. In over-thickened continental arc settings, where metamorphic reactions may dominate, the crust may not show

the same isotopic stratification observed in thin oceanic arcs composed of igneous cumulates (e.g., Central Aleutians: Sosa et al., 2024).

## 6. Conclusions

Iron isotope analyses of lower to mid/upper-crustal xenoliths from the Mercaderes region of the Colombian Andes reveals a narrow compositional range of  $\delta^{56}\text{Fe} = -0.02$  to  $+0.11\text{‰}$ . The  $\delta^{56}\text{Fe}$  of mid to upper-crustal diorites ( $\delta^{56}\text{Fe} = +0.05$  to  $+0.06\text{‰}$ ) overlaps the range observed in the lower-crustal garnet clinopyroxenites ( $\delta^{56}\text{Fe} = -0.02$  to  $+0.07\text{‰}$ ), implying that, at least regionally, the Fe isotope composition of the Andean crust ~70 to 21 km below the surface is not vertically stratified. This is inconsistent with previous theories and thermodynamically-based fractional crystallization modeling, which suggest that extensive garnet clinopyroxenite crystallization from primitive arc basalts should form an isotopically low  $\delta^{56}\text{Fe}$  crustal root. The lack of correlation between the lithology of the Mercaderes xenoliths and their Fe isotope ratio, major element composition, or trace element composition is also inconsistent with a purely cumulate origin. Our preferred explanation for the Fe isotope data is that the Mercaderes suite represents a prograde metamorphic sequence in which amphibole dehydration reactions drive the densification of diorite cumulates to form garnet clinopyroxenite residues. As our data are limited to “low-MgO” garnet clinopyroxenites (i.e., MgO < 13 wt.%), they do not

preclude the formation of clinopyroxene-rich high-MgO garnet clino-pyroxenites at the base of the Andean crust through igneous processes. Rather, we suggest garnet pyroxenite suites from thick arcs may represent an amalgamation of igneous and metamorphic processes acting concurrently. Primitive basaltic melts may fractionate high-MgO garnet clinopyroxenite cumulates at the base of the crust before rising to crystallize mid/upper-crustal diorite or gabbros. Partial melting and densification of the high-MgO pyroxenite root and mid/upper-crustal diorite protoliths in response to crustal shortening and burial may act in tandem to promote lower-crustal delamination in a self-feeding mechanism. Fe isotopes provide a promising tool to disentangle igneous and metamorphic processes and should receive greater attention in future studies of lower-crustal structure and chemistry.

### CRediT authorship contribution statement

**Emma S. Sosa:** Writing – original draft, Visualization, Investigation, Formal analysis, Conceptualization. **Claire E. Bucholz:** Writing – review & editing, Funding acquisition, Conceptualization. **Juan David Hernández-Montenegro:** Writing – review & editing, Formal analysis. **Andrés Rodriguez-Vargas:** Writing – review & editing, Resources. **Michael A. Kipp:** Writing – review & editing, Formal analysis. **François L.H. Tissot:** Writing – review & editing, Supervision, Resources.

### Declaration of competing interest

The authors declare that they have no known competing financial interests or personal relationships that could have appeared to influence the work reported in this paper.

### Acknowledgments

We thank C. Ma (Caltech) for assistance with the EMPA, T.M. Present (Caltech) for his help with XRF spectroscopy, O. Wilner (Caltech) for help with the ICP-MS, R. Grigoryan (Caltech) for support with the Neptune, and K. McCarty (Pomona) and N.F. Dalleska (Caltech) for their help with LA-ICP-MS. We thank P. Asimow and J. Eiler for their helpful discussion during the course of this work. This work was supported by NSF grant EAR 1943629 awarded to C. Bucholz. E. Sosa was supported by the National Science Foundation Graduate Research Fellowship under grant DGE-1745301. We thank Fang-Zhen Teng for editorial handling of our manuscript. This manuscript was significantly improved by thoughtful and constructive reviews from E. Cottrell and one anonymous reviewer.

### Supplementary materials

Supplementary material associated with this article can be found, in the online version, at [doi:10.1016/j.epsl.2024.119050](https://doi.org/10.1016/j.epsl.2024.119050).

### Data availability

All original data are available in the supplementary materials.

### References

- Alonso Perez, R. (2007). The role of garnet in the evolution of hydrous, calc-alkaline magmas: an experimental study at 0.8–1.5 GPa (Doctoral dissertation, ETH Zurich).
- Anderson, J.L., Smith, D.R., 1995. The effects of temperature and  $f_{\text{O}_2}$  on the Al-in-hornblende barometer. *Am. Mineral.* 80 (5–6), 549–559.
- Beard, B.L., Johnson, C.M., 2004. Fe isotope variations in the modern and ancient earth and other planetary bodies. *Rev. Mineral. Geochem.* 55 (1), 319–357.
- Beyer, C., Frost, D.J., Miyajima, N., 2015. Experimental calibration of a garnet-clinopyroxene geobarometer for mantle eclogites. *Contrib. Mineral. Petro.* 169, 1–21.
- Bird, P., 1979. Continental delamination and the Colorado Plateau. *J. Geophys. Res.* 84 (B13), 7561–7571.
- Blatter, D.L., Sisson, T.W., Hankins, W.B., 2013. Crystallization of oxidized, moderately hydrous arc basalt at mid-to-lower-crustal pressures: implications for andesite genesis. *Contrib. Mineral. Petro.* 166, 861–886.
- Blatter, D.L., Sisson, T.W., Hankins, W.B., 2023. Garnet stability in arc basalt, andesite, and dacite - an experimental study. *Contrib. Mineral. Petro.* 178 (6), 33.
- Bloch, E., Ibañez-Mejia, M., Murray, K., Vervoort, J., Müntener, O., 2017. Recent crustal foundering in the Northern Volcanic Zone of the Andean arc: petrological insights from the roots of a modern subduction zone. *Earth Planet. Sci. Lett.* 476, 47–58.
- Blundy, J.D., Falloon, T.J., Wood, B.J., Dalton, J.A., 1995. Sodium partitioning between clinopyroxene and silicate melts. *J. Geophys. Res.* 100 (B8), 15501–15515.
- Bowman, E.E., Ducea, M.N., Triantafyllou, A., 2021. Arclogites in the subarc lower crust: effects of crystallization, partial melting, and retained melt on the foundering ability of residual roots. *J. Petrol.* 62 (12), egab094.
- Bryant, J.A., Yodzinski, G.M., Hall, M.L., Lewicki, J.L., Bailey, D.G., 2006. Geochemical constraints on the origin of volcanic rocks from the Andean Northern Volcanic Zone, Ecuador. *J. Petrol.* 47 (6), 1147–1175.
- Bucholz, C.E., Spencer, C.J., 2019. Strongly peraluminous granites across the Archean-Proterozoic transition. *J. Petrol.* 60 (7), 1299–1348.
- Cooper, G.F., Davidson, J.P., Blundy, J.D., 2016. Plutonic xenoliths from Martinique, Lesser Antilles: evidence for open system processes and reactive melt flow in island arc crust. *Contrib. Mineral. Petro.* 171, 1–21.
- Craddock, P.R., Dauphas, N., 2010. Iron isotopic compositions of geological reference materials and chondrites. *Geostand. Geoanal. Res.* 35 (1), 101–123.
- Daczko, N.R., Clarke, G.L., Klepeis, K.A., 2001. Transformation of two-pyroxene hornblende granulite to garnet granulite involving simultaneous melting and fracturing of the lower crust, Fiordland, New Zealand. *J. Metamorph. Geol.* 19 (5), 549–562.
- Dauphas, N., Janney, P.E., Mendybaev, R.A., Wadhwa, M., Richter, F.M., Davis, A.M., Foley, C.N., 2004. Chromatographic separation and multicollection-ICPMS analysis of iron. Investigating mass-dependent and-independent isotope effects. *Anal. Chem.* 76 (19), 5855–5863.
- Dauphas, N., Pourmand, A., Teng, F.Z., 2009. Routine isotopic analysis of iron by HR-MC-ICPMS: how precise and how accurate? *Chem. Geol.* 267 (3–4), 175–184.
- Dauphas, N., Roskosz, M., Alp, E.E., Neuville, D.R., Hu, M.Y., Sio, C.K., Cordier, C., 2014. Magma redox and structural controls on iron isotope variations in Earth's mantle and crust. *Earth Planet. Sci. Lett.* 398, 127–140.
- Dodge, F.C.W., Lockwood, J.P., Calk, L.C., 1988. Fragments of the mantle and crust from beneath the Sierra Nevada batholith: xenoliths in a volcanic pipe near Big Creek, California. *Geol Soc Am Bull* 100 (6), 938–947.
- Du, D.H., Tang, M., Li, W., Kay, S.M., Wang, X.L., 2022. What drives Fe depletion in calc-alkaline magma differentiation: insights from Fe isotopes. *Geology* 50 (5), 552–556.
- Ducea, M., Saleeby, J., 1998. A case for delamination of the deep batholithic crust beneath the Sierra Nevada, California. *Int. Geol. Rev.* 40 (1), 78–93.
- Ducea, M.N., Chapman, A.D., Bowman, E., Balica, C., 2021b. Arclogites and their role in continental evolution; part 2: relationship to batholiths and volcanoes, density and foundering, remelting and long-term storage in the mantle. *Earth. Sci. Rev.* 214, 103476.
- Ducea, M.N., Chapman, A.D., Bowman, E., Triantafyllou, A., 2021a. Arclogites and their role in continental evolution; part 1: background, locations, petrography, geochemistry, chronology and thermobarometry. *Earth. Sci. Rev.* 214, 103375.
- Erdman, M.E., Lee, C.T.A., Levander, A., Jiang, H., 2016. Role of arc magmatism and lower crustal foundering in controlling elevation history of the Nevadaplano and Colorado Plateau: A case study of pyroxenite lower crust from central Arizona, USA. *EPSL* 439, 48–57.
- Gianola, O., Costa, B., Ferri, F., Gilio, M., Petrelli, M., Murri, M., Cesare, B., 2023. Melt inclusions in arclogitic xenoliths constrain the genesis of the lower continental arc crust beneath the Northern Volcanic Zone, Colombia. *J. Petrol.* 64 (6), egad038.
- Graham, C.M., Powell, R., 1984. A garnet-hornblende geothermometer: calibration, testing, and application to the Pelona Schist, Southern California. *J. Metamorph. Geol.* 2 (1), 13–31.
- Green, T.H., Ringwood, A.E., 1968. Genesis of the calc-alkaline igneous rock suite. *Contrib. Mineral. Petro.* 18 (2), 105–162.
- Greene, A.R., DeBari, S.M., Kelemen, P.B., Blusztajn, J., Clift, P.D., 2006. A detailed geochemical study of island arc crust: the Talkeetna 'tion, south-central Alaska. *J. Petrol.* 47 (6), 1051–1093.
- Hawthorne, F.C., Oberti, R., Harlow, G.E., Maresch, W.V., Martin, R.F., Schumacher, J.C., Welch, M.D., 2012. Nomenclature of the amphibole supergroup. *Am. Mineral.* 97 (11–12), 2031–2048.
- Holland, T., Blundy, J., 1994. Non-ideal interactions in calcic amphiboles and their bearing on amphibole-plagioclase thermometry. *Contrib. Mineral. Petro.* 116, 433–447.
- Holycross, M., Cottrell, E., 2023. Garnet crystallization does not drive oxidation at arcs. *Science* (1979) 380 (6644), 506–509.
- Jagoutz, O., Müntener, O., Burg, J.P., Ulmer, P., Jagoutz, E., 2006. Lower continental crust formation through focused flow in km-scale melt conduits: the zoned ultramafic bodies of the Chilas Complex in the Kohistan Island arc (NW Pakistan). *Earth Planet. Sci. Lett.* 242 (3–4), 320–342.
- Jagoutz, O., Müntener, O., Schmidt, M.W., Burg, J.P., 2011. The roles of flux-and decompression melting and their respective fractionation lines for continental crust formation: evidence from the Kohistan arc. *Earth Planet. Sci. Lett.* 303 (1–2), 25–36.
- Jagoutz, O.E., Burg, J.P., Hussain, S., Dawood, H., Pettke, T., Iizuka, T., Maruyama, S., 2009. Construction of the granitoid crust of an island arc part I: geochronological and geochemical constraints from the plutonic Kohistan (NW Pakistan). *Contrib. Mineral. Petro.* 158, 739–755.
- Jull, M., Kelemen, P.Á., 2001. On the conditions for lower crustal convective instability. *J. Geophys. Res.* 106 (B4), 6423–6446.

- Kay, R.W., Kay, S.M., 1991. Creation and destruction of lower continental crust. *Geologische Rundschau* 80, 259–278.
- Kay, R.W., Kay, S.M., 1993. Delamination and delamination magmatism. *Tectonophysics*, 219 (1–3), 177–189.
- Kay, S.M., Coira, B., Viramonte, J., 1994. Young mafic back arc volcanic rocks as indicators of continental lithospheric delamination beneath the Argentine Puna plateau, central Andes. *J. Geophys. Res.* 99 (B12), 24323–24339.
- Lee, C.T.A., Anderson, D.L., 2015. Continental crust formation at arcs, the arclogite “delamination” cycle, and one origin for fertile melting anomalies in the mantle. *Sci. Bull. (Beijing)* 60 (13), 1141–1156.
- Lee, C.T.A., Cheng, X., Horodyskyj, U., 2006. The development and refinement of continental arcs by primary basaltic magmatism, garnet pyroxenite accumulation, basaltic recharge and delamination: insights from the Sierra Nevada, California. *Contrib. Mineral. Petrol.* 151, 222–242.
- Lewis, M.J., Bucholz, C.E., Jagoutz, O.E., 2021. Evidence for polybaric fractional crystallization in a continental arc: hidden Lakes mafic complex, Sierra Nevada batholith, California. *Contrib. Mineral. Petrol.* 176, 1–27.
- Lewis, M.J., Ryan-Davis, J.R., Bucholz, C.E., 2023. Mafic intrusions record mantle inputs and crustal thickness in the eastern Sierra Nevada batholith, California, USA. In: *Geol. Soc. Am. Bull.*, 136, pp. 1808–1826.
- Li, D.Y., Xiao, Y.L., Li, W.Y., Zhu, X., Williams, H.M., Li, Y.L., 2016. Iron isotopic systematics of UHP eclogites respond to oxidizing fluid during exhumation. *J. Metamorph. Geol.* 34 (9), 987–997.
- Liang, W., Huang, J., Zhang, G., Huang, F., 2022. Iron isotopic fractionation during eclogite anatexis and adakitic melt evolution: insights into garnet effect on Fe isotopic variations in high-silica igneous rocks. *Contrib. Mineral. Petrol.* 177 (3), 33.
- Mpodozis, C., Kay, S.M., 1992. Late Paleozoic to Triassic evolution of the Gondwana margin: evidence from Chilean Frontal Cordilleran batholiths (28°S to 31°S). In: *Geol. Soc. Am. Bull.*, 104, pp. 999–1014.
- Müntener, O., Ulmer, P., 2018. Arc crust formation and differentiation constrained by experimental petrology. *Am. J. Sci.* 318 (1), 64–89.
- Nandedkar, R.H., Ulmer, P., Müntener, O., 2014. Fractional crystallization of primitive, hydrous arc magmas: an experimental study at 0.7 GPa. *Contrib. Mineral. Petrol.* 167 (6), 1015.
- Nie, N.X., Dauphas, N., Alp, E.E., Zeng, H., Sio, C.K., Hu, J.Y., Spear, F.S., 2021. Iron, magnesium, and titanium isotopic fractionations between garnet, ilmenite, fayalite, biotite, and tourmaline: results from NRIXS, ab initio, and study of mineral separates from the Moosilauke metapelite. *Geochim. Cosmochim. Acta* 302, 18–45.
- Ravna, K., 2000. The garnet-clinopyroxene  $\text{Fe}^{2+}$ -Mg geothermometer: an updated calibration. *J. Metamorph. Geol.* 18 (2), 211–219.
- Ridolfi, F., 2021. Amp-TB2: an updated model for calcic amphibole thermobarometry. *Minerals* 11 (3), 324.
- Ringuette, L., Martignole, J., Windley, B.F., 1999. Magmatic crystallization, isobaric cooling, and decompression of the garnet-bearing assemblages of the Jijal sequence (Kohistan terrane, western Himalayas). *Geology*, 27 (2), 139–142.
- Rodríguez-Vargas, A., Koester, E., Mallmann, G., Conceição, R.V., Kawashita, K., Weber, M.B.I., 2005. Mantle diversity beneath the Colombian Andes, northern volcanic zone: constraints from Sr and Nd Isotopes. *Lithos*, 82 (3–4), 471–484.
- Rubatto, D., Burger, M., Lanari, P., Hattendorf, B., Schwarz, G., Neff, C., Günther, D., 2020. Identification of growth mechanisms in metamorphic garnet by high-resolution trace element mapping with LA-ICP-TOFMS. *Contrib. Mineral. Petrol.* 175 (7), 61.
- Rudnick, R.L., Fountain, D.M., 1995. Nature and composition of the continental crust: a lower crustal perspective. *Rev. Geophys.* 33 (3), 267–309.
- Saleeby, J., Ducea, M., Clemens-Knott, D., 2003. Production and loss of high-density batholithic root, southern Sierra Nevada, California. *Tectonics*, 22 (6).
- Sawyer, E.W., 2014. The inception and growth of leucosomes: microstructure at the start of melt segregation in migmatites. *J. Metamorph. Geol.* 32 (7), 695–712.
- Sen, C., Dunn, T., 1994. Dehydration melting of a basaltic composition amphibolite at 1.5 and 2.0 GPa: implications for the origin of adakites. *Contrib. Mineral. Petrol.* 117 (4), 394–409.
- Sosa, E.S., Bucholz, C.E., Hernández-Montenegro, J.D., Kipp, M.A., Tissot, F.L., Ratschbacher, B.C., Kay, R.W., 2024. Lower crustal control in the iron isotope systematics of plutonic xenoliths from Adak Island, Central Aleutians, with implications for arc magma geochemistry. *Geochim. Cosmochim. Acta* 377, 1–18.
- Spear, F.S., Silverstone, J., 1983. Quantitative PT paths from zoned minerals: theory and tectonic applications. *Contrib. Mineral. Petrol.* 83 (3–4), 348–357.
- Stowell, H., Tulloch, A., Zuluaga, C., Koenig, A., 2010. Timing and duration of garnet granulite metamorphism in magmatic arc crust, Fiordland, New Zealand. *Chem. Geol.* 273 (1–2), 91–110.
- Tang, M., Erdman, M., Eldridge, G., Lee, C.T.A., 2018. The redox “filter” beneath magmatic orogens and the formation of continental crust. *Sci. Adv.* 4 (5), eaar4444.
- Ulmer, P., Kaegi, R., Müntener, O., 2018. Experimentally derived intermediate to silicic-rich arc magmas by fractional and equilibrium crystallization at 1·0 GPa: an evaluation of phase relationships, compositions, liquid lines of descent and oxygen fugacity. *J. Petrol.* 59 (1), 11–58.
- Vigneresse, J.L., Barbey, P., Cuney, M., 1996. Rheological transitions during partial melting and crystallization with application to felsic magma segregation and transfer. *J. Petrol.* 37 (6), 1579–1600.
- Villiger, S., Ulmer, P., Müntener, O., 2007. Equilibrium and fractional crystallization experiments at 0·7 GPa; the effect of pressure on phase relations and liquid compositions of tholeiitic magmas. *J. Petrol.* 48 (1), 159–184.
- Villiger, S., Ulmer, P., Müntener, O., Thompson, A.B., 2004. The liquid line of descent of anhydrous, mantle-derived, tholeiitic liquids by fractional and equilibrium crystallization—an experimental study at 1·0 GPa. *J. Petrol.* 45 (12), 2369–2388.
- Weber, M.B., Tarney, J., Kempton, P.D., Kent, R.W., 2002. Crustal make-up of the northern Andes: evidence based on deep crustal xenolith suites, Mercaderes, SW Colombia. *Tectonophysics*, 345 (1–4), 49–82.
- Weber, M.B.I., 1998. The Mercaderes Río Mayo xenoliths, Colombia: Their bearing on mantle and crustal processes in the Northern Andes. University of Leicester (United Kingdom). PhD thesis.
- Williams, H.M., Peslier, A.H., McCammon, C., Halliday, A.N., Levasseur, S., Teutsch, N., Burg, J.P., 2005. Systematic iron isotope variations in mantle rocks and minerals: the effects of partial melting and oxygen fugacity. *Earth Planet. Sci. Lett.* 235 (1–2), 435–452.
- Wolf, M.B., Wyllie, P.J., 1991. Dehydration-melting of solid amphibolite at 10 kbar: textural development, liquid interconnectivity and applications to the segregation of magmas. *Mineral. Petrol.* 44 (3–4), 151–179.
- Wyllie, P.J., Wolf, M.B., 1993. Amphibolite dehydration-melting: sorting out the solidus. *Geol. Soc., Lond., Spec. Publ.* 76 (1), 405–416.
- Yamamoto, H., Yoshino, T., 1998. Superposition of replacements in the mafic granulites of the Jijal complex of the Kohistan arc, northern Pakistan: dehydration and rehydration within deep arc crust. *Lithos*, 43 (4), 219–234.
- Yoshino, T., Satish-Kumar, M., 2001. Origin of scapolite in deep-seated metagabbros of the Kohistan Arc, NW Himalayas. *Contrib. Mineral. Petrol.* 140 (5), 511–531.
- Zhao, G., Cawood, P.A., Wilde, S.A., Lu, L., 2001. High-pressure granulites (retrograded eclogites) from the Hengshan Complex, North China Craton: petrology and tectonic implications. *J. Petrol.* 42 (6), 1141–1170.
- Zieman, L., Ibañez-Mejia, M., Rooney, A.D., Bloch, E., Pardo, N., Schoene, B., Szymanowski, D., 2023. To sink, or not to sink: the thermal and density structure of the modern northern Andean arc constrained by xenolith petrology. *Geology*, 51 (6), 586–590.
- Zieman, L.J., Ibañez-Mejia, M., Tissot, F.L., Tompkins, H.G., Pardo, N., Bloch, E.M., 2024. Zirconium stable isotope fractionation during intra-crustal magmatic differentiation in an active continental arc. *Geochim. Cosmochim. Acta* 365, 53–69.